water

MDPI

Article

Pre-Messinian Deposits of the Mediterranean Ridge: Biostratigraphic and Geochemical Evidence from the Olimpi Mud Volcano Field

Anastasios Nikitas [1,2,3], Maria V. Triantaphyllou [1,*], Grigoris Rousakis [2], Ioannis Panagiotopoulos [1,2], Nikolaos Pasadakis [4], Ioannis Hatzianestis [2] and Alexandra Gogou [2]

[1] Faculty of Geology and Geoenvironment, School of Science, National and Kapodistrian University of Athens, University Campus, 15784 Zografou, Greece; anikitas@geol.uoa.gr (A.N.); ioapanag@geol.uoa.gr (I.P.)
[2] Hellenic Centre for Marine Research, Institute of Oceanography, 46.7 km Athens-Sounio Ave., 19013 Anavyssos, Greece; rousakis@hcmr.gr (G.R.); jhat@hcmr.gr (I.H.); agogou@hcmr.gr (A.G.)
[3] School of Geology, Aristotle University of Thessaloniki, 54124 Thessaloniki, Greece
[4] Institute of Petroleum Research (IPR)—FORTH, University Campus, 73100 Chania, Greece; pasadaki@mred.tuc.gr
* Correspondence: mtriant@geol.uoa.gr; Tel.: +30-2107274893

Abstract: This study presents the results derived from micropaleontological and organic geochemical analyses of mud breccia samples obtained (through gravity coring) from five mud volcanoes (Gelendzhik, Heraklion, Moscow, Milano, Leipzig) located at the Olimpi mud volcano field on the Mediterranean Ridge accretionary complex. A thorough calcareous nannofossil semi-quantitative analysis was performed to determine the biostratigraphic assignment of the deep-seated source strata. Mudstone/shale clasts of different stratigraphic levels were identified and assigned to the Miocene nannofossil biozones CNM10, CNM8–9, CNM7, CNM6–7, and Oligocene CNO4/CNO5. A single mudstone clast from the Gelendzhik plateau, assigned to the biozone CNM10, demonstrated unique micropaleontological and geochemical characteristics, suggesting a sapropelic origin. Subsequently, the total organic carbon (TOC) content and thermal maturity of the collected mud breccias was evaluated using the Rock-Eval pyrolysis technique, and their oil and gas potential was estimated. The pyrolyzed sediments were both organic rich and organic poor (TOC >0.5% or <0.5%, respectively), with their organic matter showing characteristics of the type III kerogen that consists of adequate hydrogen to be gas generative, but insufficient hydrogen to be oil prone. However, the organic matter of the late Serravallian (CNM10) sapropelic mudstone was found to consist of a mixed type II/III kerogen, implying an oil-prone source rock.

Keywords: mud breccia; calcareous nannofossil analysis; biozone; Rock-Eval pyrolysis; offshore southern Crete Island

Citation: Nikitas, A.; Triantaphyllou, M.V.; Rousakis, G.; Panagiotopoulos, I.; Pasadakis, N.; Hatzianestis, I.; Gogou, A. Pre-Messinian Deposits of the Mediterranean Ridge: Biostratigraphic and Geochemical Evidence from the Olimpi Mud Volcano Field. *Water* **2021**, *13*, 1367. https://doi.org/10.3390/w13101367

Academic Editors: Serafeim E. Poulos, Vasilios Kapsimalis and Ioannis P. Panagiotopoulos

Received: 13 March 2021
Accepted: 10 May 2021
Published: 14 May 2021

1. Introduction and Geotectonic Setting

Mud volcanoes (MVs) are very common structures on the eastern Mediterranean seafloor, distributed in areas under a compressional tectonic regime. In total, more than 250 MVs have been identified on the Mediterranean ridge (MR), while such structures are absent throughout the neighboring tectonically inactive Hellenic backstop, even though extensional stresses may prevail in places. MVs are considered as the most important pathways for the release of overpressure caused primarily by tectonic movements and secondarily by the production of diagenetic fluids (biogenic and/or thermogenic) within deep-seated sediments.

Many studies have been carried out during the past decades in order to determine the MVs' spatial distribution in the eastern Mediterranean basin (Figure 1) (e.g., [1–5]),

their sedimentological and geochemical characteristics [6–10], and their possible relation to gas hydrates and gas seeps [11–15].

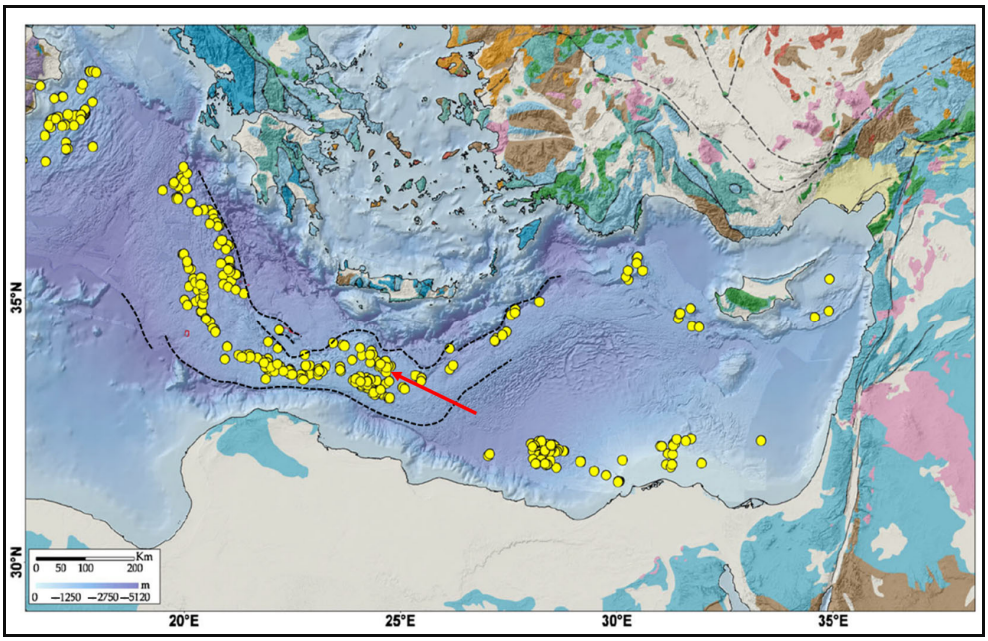

Figure 1. Spatial distribution of the mud volcanoes (see the yellow bullets) in the eastern Mediterranean basin. The thick dashed lines indicate the northern and southern boundaries of the central Mediterranean Ridge, while the red arrow indicates the approximate location of the Olimpi mud volcano field. Modified from Mascle et al. [5]; see [16] for the explanation of the additional information shown on the map.

Based on Mediterranean Sea studies, the sediments extruded during the eruptive activity of MVs comprise mixtures of a poorly sorted clayey, silty, and sandy matrix along with angular to round coarser material (i.e., pebbles, cobbles, or even larger clasts), which usually do not share the same stratigraphic origin. The established term for these sediments is "mud breccia". Cita et al. [17] were the first authors to use the previous term aiming to describe the material expelled from the Prometheus MV, which consists of a grey clay- and silt-sized matrix supporting centimeter-sized sub-rounded clasts of semi-indurated sediment [18].

The Olimpi mud volcano field (OMVF) is located on the central-northern MR (Figure 1) and includes several mud domes/complexes. The MR is a relatively deep (~1700–2000 m) and a wide ridge on the bed of the eastern Mediterranean Sea, running along an area extending from Calabria, south of Crete Island, to the southwest edge of the Turkish coast, and from there, eastwards south of Cyprus Island. The MR is being uplifted by compressional stresses, triggered by the collision and subsequent subduction of the African plate beneath the Eurasian, Aegean, and Anatolian plates. Hence, the MR is actually the accretionary wedge/prism of this subduction zone, while the marine region offshore of southern Crete is considered as a forearc basin (e.g., [19,20]. The compressional tectonic regime developed in the MR consists of the latest event of the cyclic tectono-metamorphic process that took place during the migration of the Hellenic orogenic belt towards the most external (southern) units [19,21]. A thick continental crust developed because of the stacking of the Cretan nappe piles (e.g., Mani/Plattenkalk, Arna/Phyllites-Quartzites, Gavrovo, Pindos) during the Oligocene–early Miocene under a N-S trending compressional deformation [22].

During the Miocene–Pliocene, the lithospheric plate convergence zone and, subsequently, the tectonic compression migrated southwards to the Mediterranean region

offshore of southern Crete and offshore of southern Peloponnese [23]. As a result, the compression in the Mediterranean basin led to the onset of the MR development. At the same time, Crete and Peloponnese, which previously experienced compressional stresses, were subjected to a N-S trending extensional tectonic regime. In the Miocene–early Pliocene, crustal extension in Crete caused the uplifting of the lower nappes [22,24], and sedimentary basins were developed onshore and offshore (backstop area) Crete and Peloponnese.

The mud volcanism is most probably related to backthrusting processes along the northern boundary of the accretionary wedge, near the Hellenic backstop region [25]. The ongoing (since Miocene–Pliocene) tectonic compressional deformation in the MR has been considered as the triggering process for the development of MVs since the early Pleistocene. For example, the first eruptive activity of the Napoli MV was estimated between 1.25 and 1.5 Ma, while the first eruption of the Milano MV was estimated at 1.75 Ma [6,7].

The sediments extruded onto the seafloor during the MV eruptions may originate from sub-salt formations of pre-Messinian age or from source beds of the Messinian age (e.g., [10]) and consist of a mixture of clasts of variable lithology and consolidation, supported by very stiff to very soft sandy mud matrix having clay as the dominant fraction (e.g., see Appendix A in Panagiotopoulos et al. [26]). In terms of petrology, most of the clasts of the mud breccia matrices are considered to be derived from the North African passive margin, except of various ophiolite-related lithoclasts that are probably derived from higher thrust sheets of Crete [25].

The scope of the present study was to perform micropaleontological and organic geochemical analyses on mud breccia deposits obtained from five MVs (Gelendzhik, Heraklion, Moscow, Milano, and Leipzig) of the OMVF using gravity coring, in order to shed light on the deep-seated sub-salt formations of the region, since there is lack of a deep-well drilling in this particular MR area. To the best of our knowledge, the only stratigraphy in the host sediment of the OMVF, albeit very shallow, is the one provided by Cita et al. [27] through a core analysis, which revealed that the occurrence of pelagic sequences of the Holocene to Middle Pleistocene are composed mainly of marl and sapropel, as well as tephra layers as minor, isochronous lithologies.

2. Materials and Methods

2.1. Sediment Collection and Sample Treatment

The sediment cores investigated in this work were collected from the crests of the relevant MVs (see Figure 2a for coring locations and core names) and initially examined by Panagiotopoulos et al. [26]. According to the previous study, the sampling locations were selected based on the intensity of the backscatter signal recorded during a swath bathymetry survey in the OMVF (Figure 2a–c) carried out by the R/V Aegaeo in 2016. The sediment sampling was performed using a gravity corer (Benthos Inc., Massachusetts, USA) with a 3-m-long core barrel (Benthos Inc., Massachusetts, USA). Because of the highly incohesive nature of the majority of the mud breccia deposits, the recovery length of the retrieved cores was generally incomplete (70–132 cm).

In the laboratory, 100–200 g of material was initially recovered from 14 mud breccia facies (see Figure 3 and [26]) and, then, clasts were carefully removed from the sediment matrix. In total, 42 samples (14 matrices and 28 clasts) were collected and described regarding their color (using the Munsell soil color chart), distinct features (e.g., fissilities), lithology (a representative example is displayed in Figure 4), and degree of consolidation (see Tables A1–A5 in Appendix A). The degree of the sediment matrix consolidation was already determined by Panagiotopoulos et al. [26], while the consolidation degree of clasts was estimated by the present study using the empirical testing criteria referred to in Appendix A.

All samples were split in two equal halves. The first half was completely homogenized using a mortar and pestle and an amount of at least 100 mg per sample was subjected to Rock-Eval pyrolysis, while the second half was used to produce smear slides for the microscopical study of the calcareous nannofossil content, according to standard techniques [28,29].

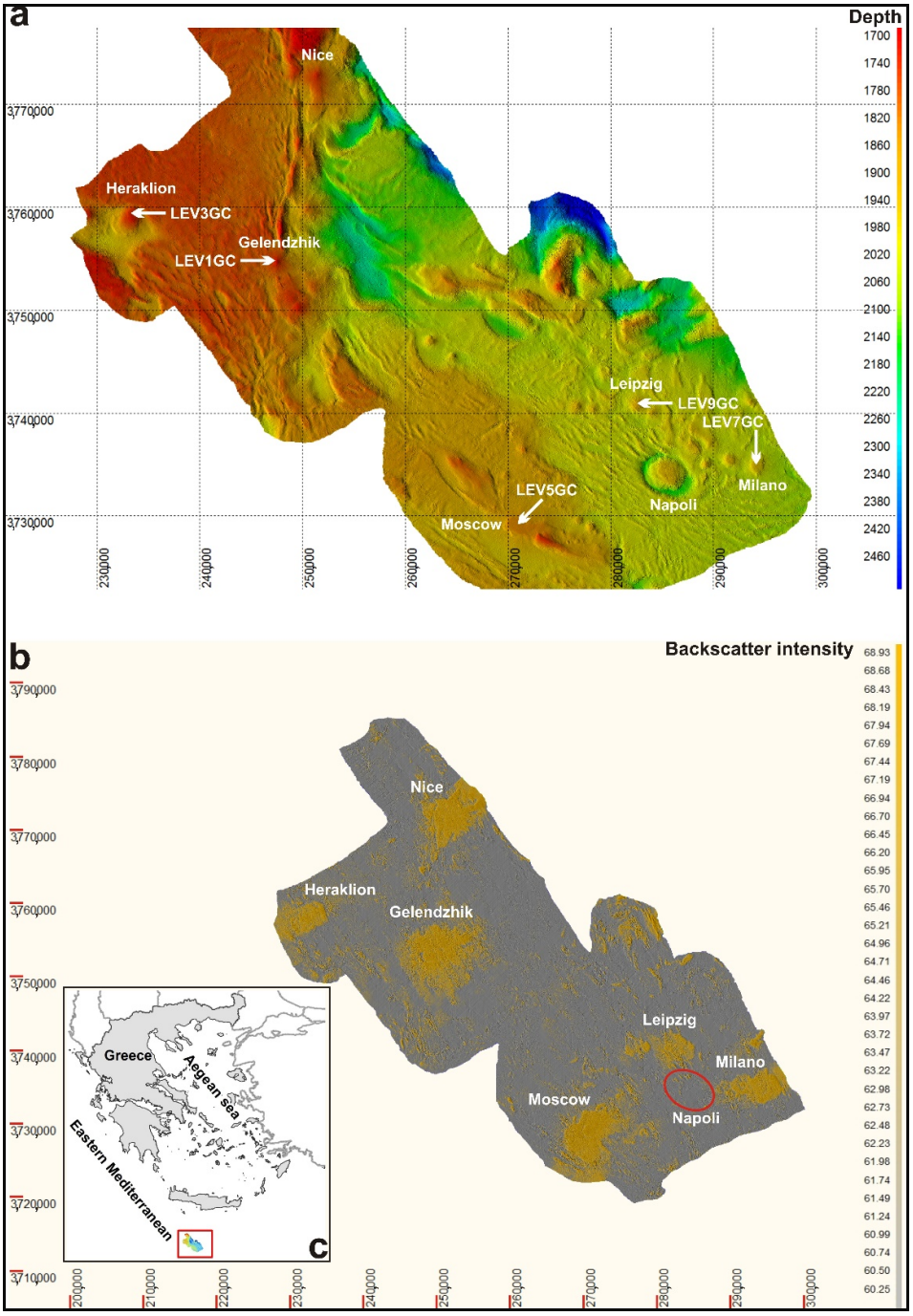

Figure 2. (**a**) Bathymetric digital terrain model of the Olimpi mud volcano field (grid interval: 50 m; ellipsoid: WGS84; projection: UTM35N; reference datum: mean sea level) and sediment coring locations (the core labels appear in white color). (**b**) Seabed reflectivity in the Olimpi mud volcano field (grid interval of 50 m), with the yellow-colored patches representing strong backscatter signal. (**c**) Location of the Olimpi mud volcano field (inset map). From Panagiotopoulos et al. [26].

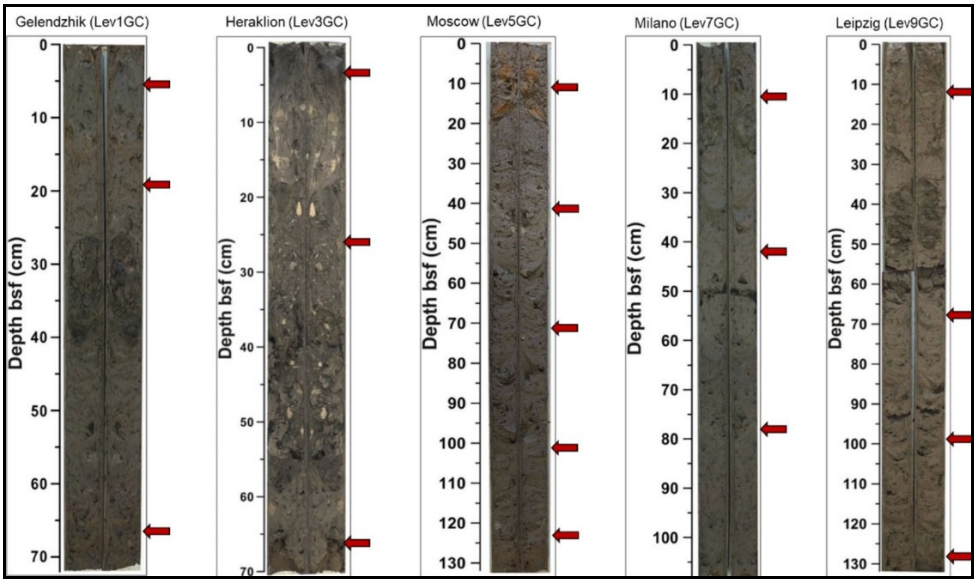

Figure 3. Images of the gravity cores recovered from the five MVs, showing the coring depth below seafloor (bsf) and the various mud breccia facies. The red arrows indicate the sampling core intervals. Modified from Panagiotopoulos et al. [26]. For a detailed description of the cored sediments see Panagiotopoulos et al. [26].

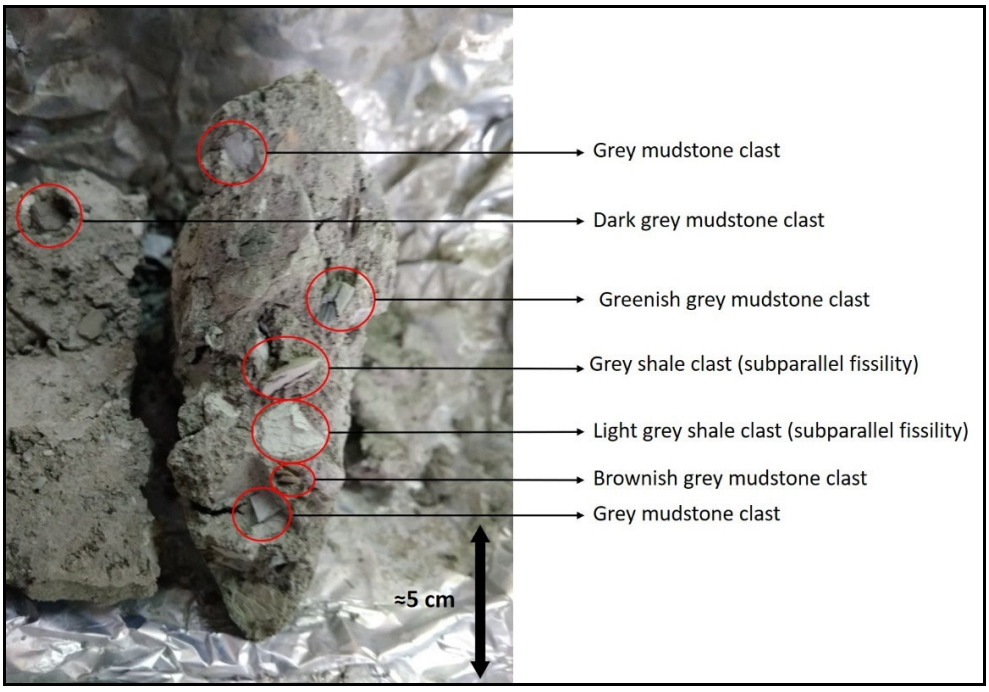

Figure 4. Image of a representative mud breccia facies from the Olimpi mud volcano field (LEV5GC core from the Moscow MV).

2.2. Micropaleontology and Biostratigraphy

Concerning the calcareous nannofossil analysis, a semi-quantitative determination was conducted in up to 300 fields of view per slide in randomly distributed longitudinal traverses using a Leica DMLSP (Leica Microsystems GmbH, Wetzlar, Germany) optical polarizing light microscope at a 1250× magnification. The traverses represented both low- and high-density material content in an effort to make accurate nannofossil determina-

tions and trace even the rarest species. The semi-quantitative abundances of the taxa encountered were recorded as follows: A, abundant: ≥1 specimen/1 field of view; C, common: ≥1 specimen/10 fields of view; F, few: 1 specimen/10–50 fields of view; R, rare: 1 specimen/>50 fields of view.

The zonal assignment follows the biostratigraphic scheme of Agnini et al. [30], which incorporates the biochronologic information from Backman et al. [31] and is correlated to the Martini [32] biozones (see Table 1).

Table 1. Biozones determined by the nannofossil study of the clast samples. The index species suggest the stratigraphic range of the samples, while the reworked species can provide valuable information about the basin's evolution. The correlation with Martini [32] biozones appears in parentheses. (*) Miocene–Pliocene species associated with potential contamination caused by the upward migration of mud breccia.

Biostratigraphic Scheme	Index Species	Main Long-Range Species (or/and Reworked)	Reworked	Samples
CNM10 (NN7)	*D. kugleri*	*C. pelagicus, C. floridanus, H. carteri, D. deflandrei, S. moriformis*	*S. disbelemnos, S. dissimilis, H. ampliaperta, S. delphix, C. abisectus, D. nodifer, R. lockeri, R. bisecta, S. ciperoensis, R. hillae, S. predistentus, Z. bijugatus, H. recta, D. lehmanii, Eiffelithus* sp. Also (*): *P. lacunosa*?, *Gephyrocapsa* sp. <3 μm	LEV1GC 4–6 clast 1, LEV1GC 4–6 clast 2, LEV1GC 65–67 clast 1, LEV5GC 100–102 clast 2
CNM8–9 (NN6)	*R. pseudoumbilicus, C. macintyrei*	*C. leptoporus, C. mesostenos, C. pelagicus, H. carteri, D. deflandrei, S. moriformis*	*S. heteromorphus, S. cometa, S. disbelemnos, R. bisecta, S. ciperoensis, D. barbadiensis, R. lockeri, R. hillae, R. reticulata, Z. bijugatus, C. fomosus, C. abisetus, C. gerrardii, R. daivesi, D. lehmanii Zeugrhabdotus* sp., *Cruciplacolithus* sp., *Eiffellithus* sp., *W. barnesiae*, undetermined Cretaceous sp. Also (*): *P. lacunosa*?, *Gephyrocapsa* <3 μm, *S. abies*	LEV1GC 18–20 clast 1, LEV7GC 40–43 clast 1, LEV7GC 40–43 clast 2 LEV7GC 78–80 clast 2, LEV9GC 10–13 clast 1, LEV9GC 98–100 clast 3, LEV9GC 128–130 clast 3
CNM7 (NN5)	*S. heteromorphus, C. miopelagicus*	*C. pelagicus, C. floridanus, D. deflandrei, S. moriformis, C. mesostenos, R. perplexa*	*R. bisecta, D. barbadiensis, W. barnesiae, Micrantholithus* sp.	LEV5GC 123–125 clast 2, LEV9GC 128–130 clast 2
CNM6–7 (NN4)	*S. heteromorphus, Helicosphaera ampliaperta*	*C. pelagicus, C. floridanus, D. deflandrei, S. moriformis, C. mesostenos, R. perplexa*	*S. cometa, S. dibelemnos, C. abisetus, R. bisecta, S. predistentus, D. barbadiensis, R. lockeri, D. lehmanii*, undetermined Cretaceous sp., *E. turriseiffelii*	LEV3GC 65–67 clast 1, LEV5GC 70–72 clast 1, LEV9GC 67–69 clast 1, LEV9GC 98–100 clast 2
CNO4/CNO5 (NP24)	*S. distentus, S. predistentus, S. ciperoensis*	*C. pelagicus, C. floridanus, D. deflandrei, S. moriformis, C. mesostenos, C. abisectus, R. bisecta, Z. bijugatus*	*D. barbadiensis, C. eopelagicus, B. parca, Eiffelithus* sp., *R. infinitus*	LEV5GC 40–42 clast 1
Assemblage mainly featuring the CNO3-CNO4/CNO 5 biozones (NP23-NP24)	*S. distentus, S. predistentus, S. peartiae*	*C. formosus, C. floridanus, D. deflandrei.*	*C. formosus, D. multiradiatus, D. barbadiensis, Arkhangelskiales* sp. Also (*): *C. miopelagicus, D. kugleri, D. discissus, D. durioi, D. exilis, H. carteri, R. pseudoumbilicus, U. jafari, S. abies*	LEV5GC 10–12 clast 1, LEV5GC 100–102 clast 1

It should be noted that sample preparation restrictions, due to the nature of the examined sediment (i.e., minute clasts within a consolidated sediment matrix), could result in the contamination of the nannofossil assemblages and organic matter content. Hence, the grinding and homogenization process of the matrix and minor clasts could artificially produce a sample characterized by various organic matter types and diverse

nannofossil assemblages. Further, the occurrence of clasts containing organic matter and nannofossils of dissimilar stratigraphic origin could be explained by the presence of an amount of residual matrix that was not sufficiently scraped off from the surface of the clasts during the sample preparation, resulting in its amalgamation with the clast.

2.3. Organic Geochemical Analysis

The samples, after being pulverized and dried at 40 °C, were subjected to the Rock-Eval pyrolysis technique [33–35] in the Institute of Petroleum Research (IPR)—FORTH, using a Delsi Rock-Eval VI system. The determined parameters are presented in Tables A1–A5 of Appendix A.

Briefly, during the Rock-Eval pyrolysis the rock sample is heated in an inert (nitrogen) atmosphere. Hydrocarbons already present in the sample are volatized at 300 °C and recorded as the S1 peak. As the analysis proceeds at higher temperatures (up to 850 °C), hydrocarbons generated from the kerogen are recorded as the S2 peak (see Figure A1 in Appendix A for representative well-defined S2 peaks), which is an indicator of thermal maturity. Carbon dioxide and carbon monoxide produced during the pyrolysis are also recorded (S3 peak). Subsequently, the residual carbon is determined during oxidation of the sample (S4 peak). Considering the experimental data, the Tmax, total organic carbon (TOC), mineral carbon (MinC) content, hydrogen index (HI = 100 × S2 × TOC^{-1}), and oxygen index (OI = 100 × S3 × TOC^{-1}) are calculated based on Emeis and Kvenvolden [36].

The HI and OI parameters are used to characterize the origin of the organic matter. Marine organisms and algae, in general, are composed of lipid- and protein-rich organic matter, where the ratio of H to C is higher than in the carbohydrate-rich constituents of land plants. HI may reach up to 600 mg g^{-1} in geological samples. OI is correlated with the ratio of O to C, which is high for polysacharride-rich remains of land plants and inert organic material (residual organic matter) encountered as background in marine sediments. OI values do not usually exceed 240 mg g^{-1}.

3. Results

3.1. General Lithological Description and Dating of Samples

The 28 examined clasts were classified as mudstones, shales, carbonate mudstones, sandstone (sample LEV9GC 67–69 clast 2), and carbonate interlaminated sandstone/mudstone (sample LEV9GC 98–100 clast 1). Mudstones, however, dominated the clast lithology. For further details, see Tables A1–A5 in Appendix A.

The14 examined sediment matrices were mixtures of clay, silt, and sand and can be classified as sandy mud. A detailed description of the mud matrices of the cored sediments in the OMVF has already been provided by Panagiotopoulos et al. [26].

Concerning the biostratigraphic dating accomplished through the calcareous nannofossil analysis (Table 1 and Tables A6–A47 in Appendix A), most of the clast samples were assigned to the early-middle Miocene (CNM6–7, CNM7, CNM8–9. and CNM10 biozones [30]). However, for the first time, Oligocene clasts (see Figure 5 and Table 1) were also identified in the broader Olimpi/Prometheus 2 area.

The rest of the clasts could not be accurately or reliably dated (see Tables A2–A5 in Appendix A) because of: (i) the significant reworking and/or mixing observed in the sediment samples; these clasts were labeled as "mixed Oligocene–Miocene"; and (ii) the lack of nannofossil content or limited occurrence of specimens (probably reworked); these clasts were labeled as "undetermined". The latter category also included the samples LEV3GC 65–67 clast 2 and LEV9GC 128–130 clast 1, due to insufficient sedimentary material for nannofossil biostratigraphic analysis.

Regarding the examined matrices, an age of mixed Oligocene–Miocene may be suggested for almost all samples, since characteristic species from completely different biozones were identified (see Tables A6, A9, A11, A14, A17, A23, A26, A29, A30, A33,

A36, A40, and A44 in Appendix A, as well as Figure 6). Only one sample (LEV3GC 2–5 matrix) appeared to be barren of nannofossils.

LEV5GC 40–42 clast 1					
Biozone: CNO4/CNO5 (NP24)					
species	A	C	F	R	specimens counted
Paleogene					
Coccolithus eopelagicus				X	2
Cyclicargolithus abisectus				X	2
Discoaster barbadiensis				X	1
Helicosphaera obliqua				X	1
Helicosphaera recta				X	2
Reticulofenestra lockeri				X	1
Reticulofenestra bisecta			X		5
Sphenolithus ciperoensis			X		4
Sphenolithus distentus				X	2
Sphenolithus predistentus				X	1
Zygrhablithus bijugatus			X		6
long range Paleogene–Neogene					
Braarudosphaera bigelowi				X	1
Coccolithus pelagicus	X				29
Coronocyclus mesostenos			X		5
Coronocyclus nitescens				X	3
Cyclicargolithus floridanus	X				81
Discoaster deflandrei		X			11
Discoaster sp.			X		3
Helicosphaera euphratis				X	2
Helicosphaera intermedia				X	3
Helicosphaera leesiae				X	2
Helicosphaera mediterranea				X	2
Pontosphaera japonica			X		6
Rhabdosphaera? sp.			X		4
Sphenolithus conicus			X		4
Sphenolithus moriformis	X				20
Cretaceous					
Broinsonia parca				X	1
Eiffelithus sp.				X	1
Rhagodiscus infinitus				X	1

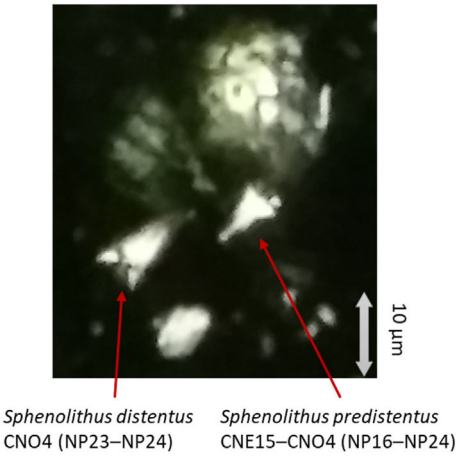

Figure 5. Example of an age-diagnostic assemblage list showing the relative abundances of the nannofossil species in the total assemblage of the LEV5GC 40–42 clast 1 sample. The coexistence of *Sphenolithus distentus* and *Sphenolithus predistentus* (their microscopic image appears at the right) and *Sphenolithus ciperoensis* defines the CNO4/CNO5 biozone. The identified Cretaceous species along with some Paleogene (pre-Oligocene) species are considered as reworked.

LEV5GC 10–12 matrix					
mixed; mostly Oligocene–Miocene					
species	A	C	F	R	specimens counted
Neogene					
Calcidiscus macintyrei			X		4
Calcidiscus premacintyrei				X	1
Coccolithus miopelagicus				X	1
Discoaster variabilis				X	1
Gephyrocapsa < 3 µm				X	2
Helicosphaera carteri				X	3
Helicosphaera orientalis				X	2
Pseudoemiliania lacunosa				X	2
Reticulofenestra pseudoumbilicus		X			9
Sphenolithus heteromorphus				X	2
Syracosphaera pulchra				X	1
Umbilicosphaera jafari			X		4
Umbilicosphaera rotula				X	1
Paleogene					
Chiasmolithus sp.				X	1
Coccolithus formosus				X	3
Cyclicargolithus abisectus				X	3
Discoaster barbadiensis				X	1
Discoaster multiradiatus				X	1
Helicosphaera recta				X	1
Reticulofenestra lockeri				X	1
Reticulofenestra hillae				X	1
Reticulofenestra stavensis				X	1
Sphenolithus ciperoensis				X	1
Sphenolithus distentus				X	1
Zygrhablithus bijugatus				X	1
long range Paleogene–Neogene					
Coccolithus pelagicus	X				11
Coronocyclus mesostenos				X	3
Cyclicargolithus floridanus			X		5
Discoaster deflandrei				X	1
Discoaster sp.			X		5
Helicosphaera intermedia				X	1
Pontosphaera multipora				X	1
Pontosphaera sp.				X	2
Reticulofenestra perplexa			X		4
small reticulofenestroids				X	3

Figure 6. Left: Example of a non-age-diagnostic assemblage list showing the relative abundances of the nannofossil species in the total assemblage of the LEV5GC 10–12 matrix sample. Right: Microscopic image of the sample indicating considerable reworking due to the concomitant occurrence of the *Calcidiscus premacintyrei* (Miocene) and *Discoaster barbadiensis* (Eocene) species. Almost all matrix samples displayed analogous microscopic images.

3.2. Organic Geochemical Analysis

The Rock-Eval analysis provides information about the richness, the quality, and the maturation level of the organic matter in sediments and rocks. Characteristic nomograms for the evaluation of the Rock-Eval experimental data are shown in Figures 7–9, according to Espitalie et al. [33], Espitalie et al. [37], Hunt [38], and Jackson et al. [39]. Samples with OI values >240 mg g^{-1} (due to both matrix mineralogy and level of organic enrichment) and/or TOC values <0.3% are not shown in Figures 7 and 8 because these data are considered of limited reliability for kerogen characterization.

3.2.1. Total Organic Carbon

The TOC values of the clasts fluctuated between 0.03% and 2.02%, while the TOC contents of the matrix samples varied between 0.25% and 0.94%. Two semi- to well-consolidated coarse-grained clasts from the Leipzig MV, i.e., one sandstone and one carbonate mudstone/sandstone (LEV9GC 67–69 clast 2 and LEV9GC 98–100 clast 1, respectively), exhibited very low values (0.03% and 0.26%, respectively), while one mudstone (LEV1GC 4–6 clast 1) from the Gelendzhik MV, dated as the middle Miocene (late Serravallian, CNM10), demonstrated the highest value.

3.2.2. Organic Matter Quality (Kerogen Type) and Thermal Maturation

Most of the data points associated with both clasts and matrices showed a distribution near the type III kerogen curve (Figures 7 and 8). Nevertheless, the organic-rich mudstone (LEV1GC 4–6 clast 1) from the Gelendzhik MV plateau (see above) may be characterized as a mixed type II/III kerogen (Figures 7 and 8).

In general, the analyzed samples were considered as "immature" for petroleum hydrocarbon generation, showing Tmax values lower than the oil window onset (Tmax of 435 °C) [33]. However, three clasts, i.e., the Miocene (CNM6–7) mudstone/carbonate mudstones LEV3GC 65–67 clast 1, LEV5GC 70–72 clast 1, and LEV9GC 67–69 clast 1, from the Heraklion, Moscow, and Leipzig MVs, respectively (see Tables A2, A3, and A5 in Appendix A, as well as Figure 8), and one mixed Oligocene–Miocene matrix sample (LEV7GC 78–80) from the Milano MV (see Table A4 in Appendix A) were nearly "mature" (Tmax of 430–434 °C). In addition, based on Figure 9, the above-mentioned mudstone (LEV1GC 4–6 clast 1) from the Gelendzhik MV could be considered as a material of "good" hydrocarbon-generation potential.

Finally, the broad scattering of the data points in the HI vs. OI plot (Figure 7) indicates multiple sources for the organic matter of the investigated mud breccias.

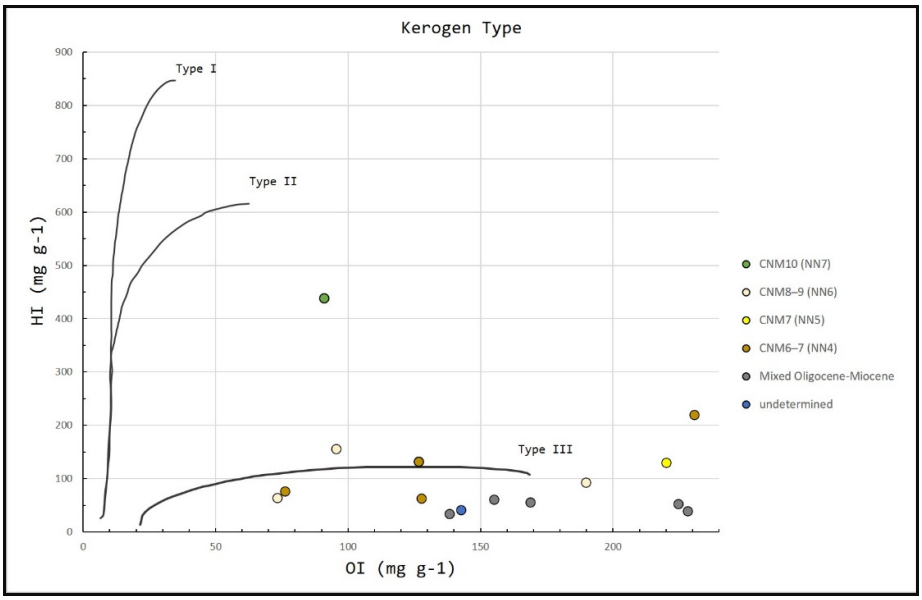

Figure 7. Modified van Krevelen diagram presenting the results of the Rock-Eval pyrolysis. One mudstone clast (LEV1GC 4–6 clast 1) dated as middle Miocene (CNM10 biozone) demonstrates different geochemical characteristics from the rest of the samples.

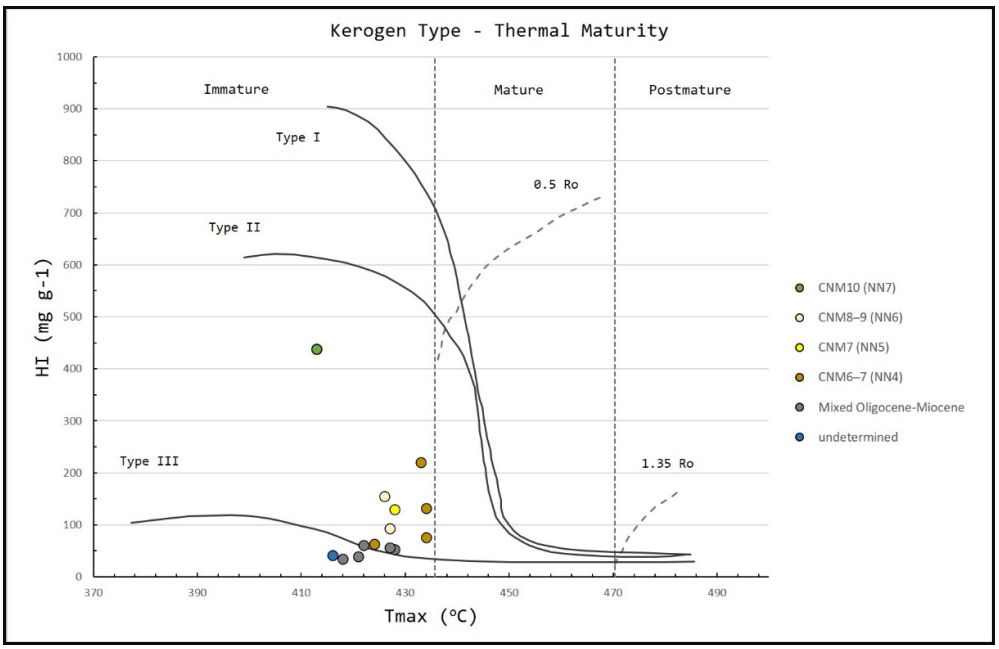

Figure 8. HI vs. Tmax plot showing, in parallel, the kerogen-type curves and maturity levels along with the upper- and lower-vitrinite reflectance thresholds (Ro) for oil generation. Note the distinct position of the sample LEV1GC 4–6 clast 1 (CNM10 biozone), which approaches the type II kerogen curve.

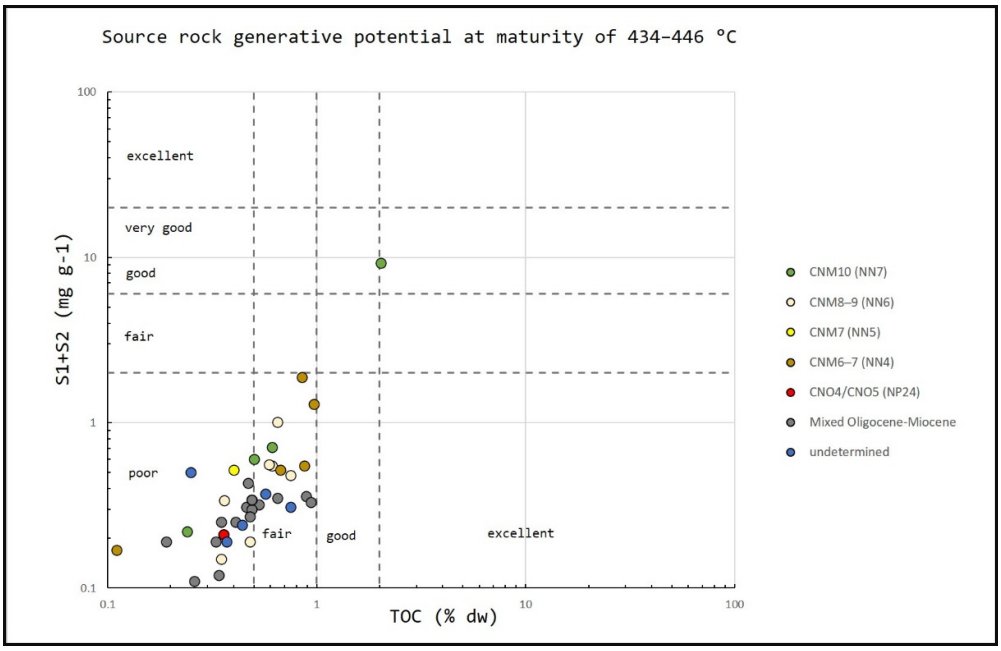

Figure 9. (S1 + S2) vs. TOC plot indicating the potential of the source rocks for hydrocarbon generation.

3.2.3. Carbonates

The MinC contents of the pyrolyzed samples were used for the calculation of the carbonate contents by applying the equation of Jiang et al. [40]: $Q_{carbonates} = 7.976 \times MinC$. According to the results (see Tables A1–A5 in Appendix A), only four clasts contained $Q_{carbonates} > 50\%$ and, thus, they were characterized as carbonate mudstones.

4. Discussion

4.1. Stratigraphic Origin Evidence

It is considered that the clasts can lead to safer conclusions regarding their stratigraphic origin compared to the mud matrices, which are rather an irregular mixture of several stratigraphic layers during their upward movement through thick sections of sedimentary rocks. In contrast, the clasts reflect more reliably the characteristics of the source rocks, because they are the result of the high consolidation of sedimentary material in the deep-seated strata that have been removed and migrated to the seabed surface because of the tectonic overpressure (related with backthrusting) developed in the region. The variability in the macroscopic characteristics of the clasts (i.e., color, fissility, grain size; see Figure 4) suggests that the clasts do not share the same stratigraphic origin. This interpretation is further supported by the microscopic observations made during the nannofossil analysis.

Previous studies have suggested that the clasts from the broader Olimpi/Prometheus 2 area should be of Burdigalian–Langhian and early Serravallian age, containing reworked Oligocene, Eocene, and Cretaceous nannofossils [6,7,41–43]. In the present study, Burdigalian–Langhian mudstone/shale clasts (assigned to biozones CNM6–7; see Table 1) were common, while the latest Serravallian and Oligocene clasts were also identified. It is worth mentioning that the newly diagnosed Oligocene clasts from the OMVF include nannofossil assemblages, which are quite similar to the typical nanno-assemblages of the age-equivalent Gavrovo flysch (e.g., [44–46]).

The LEV1GC 4–6 clast 1 sample, a mudstone from the Gelendzhik MV (see Section 3.2.1), shows some interesting features regarding both its microscopic image and geochemical values: (i) it is characterized by a great abundance of both calcareous and siliceous microfossils, which indicates increased water column primary production (e.g., [47]) by the time of sediment deposition (CNM10—latest Serravallian age); and (ii) the Rock-Eval pyrolysis of this clast showed a high TOC value (~2%) together with a high HI and a relatively low OI (438 and 91 mg g^{-1}, respectively; see Table A1 in Appendix A), which indicate low oxygen availability during the sediment deposition. Therefore, it is quite possible that anoxic/hypoxic conditions were triggered near the seafloor by the increased productivity in the euphotic zone together with enhanced organic matter preservation, resulting in the formation of deposits of sapropelic nature (e.g., [48–50]). Based on the previous interpretations, we believe that the LEV1GC 4–6 clast 1 sample originated from a sapropelic source rock.

The oldest known sapropels in the Mediterranean sedimentary sequences are considered to be of the Langhian age (~15.4 Ma) and can be found onshore northern Cyprus [51] as well as in the central part of the island, predominantly in marly successions (Kottafi Hill section, ranging up to CNM10 [52,53]). In addition, sapropel layers as old as the Langhian age (with the oldest layer assigned to the CNM7 biozone) were discovered offshore western Cyprus [54] during the leg 42A (site 375) of the Deep Sea Drilling Project (DSDP). In the latter study, a distinct sapropel was identified, whose characteristics are analogous to the LEV1GC 4–6 clast 1 sample regarding its age and organic content (~2%). Considering the fact that recent sapropels (Plio–Pleistocene and Holocene formations; e.g., [48–50,55]) are well studied and correlated across the Mediterranean basin, we suggest that the sapropel-like material of LEV1GC 4–6 clast 1 could originate from the equivalent deposits recorded in the sequences of the DSDP site 375.

Concerning the analyzed mud matrices, almost all samples were found to contain mixed assemblages consisting mostly of Miocene–Oligocene nannofossils together with older (reworked) species of Eocene and Cretaceous. The mixed assemblages in the mud matrices provide strong evidence that the investigated MVs are fed by multiple source rocks. However, one sample (LEV3GC 2–5 matrix) appeared to be barren of nannofossils (see Table A2 in Appendix A), emphasizing the great degree of heterogeneity in the mud

breccia deposit. It can be suggested that the mixing of sediments took place at two stages: (i) an initial mixing of sediments coming from different sources occurred when they entered the MV's feeder conduit and (ii) a further mixing occurred during the dynamic extrusion of the mudflows onto the seafloor.

4.2. Significance of the Reworked Nannofossil Species

Almost every examined clast included ~10% of reworked Miocene, Oligocene, Eocene, and Late- and Early-Cretaceous nannofossils, (see Tables A7, A8, A10, A12, A15, A18–A22, A24, A25, A28, A31, A32, A34, A37, A38, A41–A43, A46, and A47 in Appendix A). These reworked specimens from older strata can provide valuable information concerning the stratigraphy and geological history of the MR.

In particular, it was observed that:

- The middle Miocene (CNM7, CNM8–9 and CNM10) clasts embraced reworked nannofossils of the early-middle Miocene, Oligocene, Eocene, and Cretaceous;
- The early-middle Miocene (CNM6–7) clasts included reworked nannofossils of the Oligocene, Eocene, and Cretaceous;
- The Oligocene (CNO4/CNO5) clasts comprised reworked nannofossils of the Eocene and Cretaceous.

In addition, a remarkable observation was the absence of Paleocene species from all investigated clasts, which might be the result of severe thinning of Paleocene strata in the fold and thrust belt zone. Actually, the only indication that would support the existence of Paleocene material is the presence of *Discoaster multiradiatus*, whose first occurrence takes place at the base of CNP11 (NP9 biozone [32]).

The presence of reworked nannofossils in both Miocene and Oligocene assemblages of the analyzed clasts indicates the following: (i) subaerial/subsea exposure and erosion of Cretaceous and Eocene sequences during the Oligocene; (ii) subaerial/subsea exposure and erosion of the Oligocene, Eocene, and Cretaceous sequences during the early-middle Miocene; and (iii) subaerial/subsea exposure and erosion of the early-middle Miocene, Oligocene, Eocene, and Cretaceous sequences during the middle Miocene. It should be noted that intense sediment transport and redeposition is a common feature of the sedimentary processes in active forearc basins (e.g., formation of deep-sea flysch turbidites; see [56] and references therein).

However, it is not clear if the erosion and redeposition of the older sediments took place in subaerial or subsea conditions, even though a combination of both conditions would be more realistic. The subaerial exposure and erosion scenario can be supported by the high OI values calculated for most of the clasts after the Rock-Eval pyrolysis runs (see Tables A1–A5 in Appendix A), which is a typical characteristic of the type III kerogen that indicates high terrestrial inputs [57]. The subsea erosion scenario, e.g., caused by intense turbidity current activity, is supported by the fact that the region southern of Crete is tectonically very active and experiences both compressional and extensional stresses (e.g., [21,22]). In such environments, steep slopes are formed and frequently fail due to seismic shaking, creating favorable conditions for the development of strong turbidity currents [56].

4.3. Organic Geochemistry Evidence

From a statistical point of view, the TOC content threshold for non-reservoir shale-type (source rock) sediments in oil provinces is considered the value of 0.5% [35]. Consequently, the source rock hydrocarbon-generative potential is considered as "poor" for TOC contents <0.5%, "fair" for values of 0.5–1%, "good" for values of 1–2%, and "very good" for values greater than 2% ([58]; see Table 2). Concerning the matrix samples, only four exceeded the TOC threshold of 0.5%, while the rest of them were considered as "poor" (see Tables A1–A5 in Appendix A and Table 2). In contrast, the clast samples appeared to be richer in organic content; 12 of them appeared as "fair", while the sapro-

pelic mudstone clast (LEV1GC 4–6 clast 1) from the Gelendzhik MV plateau was classified as "very good" (TOC = 2.02%). Taking into account that the clasts can provide better evidence concerning the region's deep stratigraphy, it can be concluded that ~46% of the randomly sampled clastic material originated from Miocene source rocks of "fair" and "very good" hydrocarbon-generating potential, buried ~2 km below the MR seafloor [26].

Table 2. Source rock hydrocarbon-generation potential based on the TOC contents of the pyrolyzed sediment samples. Redrawn and modified from Peters [58].

Source Rock Generative Potential	TOC % dw	Sample Type
Poor	<0.5	10 matrices, 15 clasts
Fair	0.5–1	4 matrices, 12 clasts
Good	1–2	
Very Good	>2	1 clast

The suggested type III kerogen for the majority of analyzed samples (clasts and matrices) indicates a higher (terrestrial) plant contribution to the organic matter accumulation [57], which is in accordance with previous studies (e.g., [26,59]). Kerogen III is commonly considered as more favorable for gas enrichment than for oil generation [33]. Only the CNM10 LEV1GC 4–6 clast 1 sample, interpreted as being derived from a sapropelic formation, tended to approach the curve of the type II kerogen (see Figure 7). Kerogen II is primarily composed of marine organic materials (phytoplankton, zooplankton, and bacteria) together with allochthonous organic matter (originating, for example, from higher plants) [57] and is more prone to generating oil [33].

Based on Figure 8, all analyzed mud breccia samples were considered as "immature" to nearly "mature" for hydrocarbon-generation potential. Because the thermal condition for oil generation ranges from 100 to 150 °C [57], all cored sediments were subjected to temperatures lower than 100 °C. However, there is a possibility that four samples, i.e., LEV3GC 65–67 clast 1, LEV5GC 70–72 clast 1, LEV9GC 67–69 clast 1, and LEV7GC 78–80 matrix, which were characterized as nearly "mature" (see Section 3.2.2), were subjected to a heating close to 100 °C. Previous investigations have also led to a similar interpretation regarding the thermal maturity of clasts and matrix (e.g., [10,59], supporting the results of this study.

During the Rock-Eval pyrolysis performance, some samples demonstrated anomalous S2 signals. These anomalies concerned nine clasts (LEV1GC 4–6 clast 2, LEV1GC 18–20 clast 1, LEV1GC 65–67 clast 1, LEV5GC 10–12 clast 2, LEV5GC 40–42 clast 2, LEV5GC 123–125 clast 1, LEV5GC 123–125 clast 2, LEV7GC 40–43 clast 1, and LEV9GC 67–69 clast 2) and two matrix samples (LEV1GC 65–67 and LEV3GC 2–5), and appeared as bimodal S2 peaks (Figure 10a–d), probably indicating mixtures of organic matter from dissimilar stratigraphic horizons, from contrasting environments (terrestrial and marine), or of different thermal maturity. For this reason, the Tmax values estimated from the peaks of the S2 profiles of these samples were considered as highly uncertain; according to Yang and Horsfield [60], numerous factors can artificially modify the Tmax values and influence the maturity judgments. Nevertheless, the moderate to major reworking of the nannofossil assemblages of most of the above-mentioned clasts supports the interpretation of the organic matter mixing.

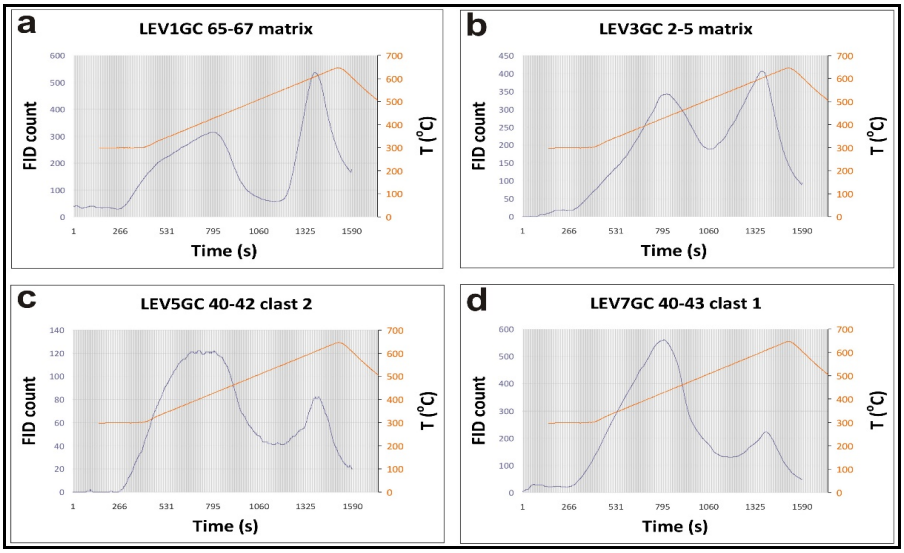

Figure 10. Distinct bimodal S2 peaks in the Rock-Eval pyrograms of samples from: (**a**) the Gelendzhik MV, (**b**) the Heraklion MV, (**c**) the Moscow MV, and (**d**) the Milano MV.

5. Conclusions

This study provides important information concerning the (pre-Messinian) sub-salt sediments of the eastern Mediterranean basin, south of Crete, which is an underexplored marine region lacking deep exploratory wells.

A biostratigraphic dating of mud breccia deposits (including clasts and mud matrices) from the Olimpi mud volcano field, based on a meticulous calcareous nannofossil analysis, led, for the first time, to the determination of one Oligocene (CNO4/CNO5) mudstone clast, two Oligocene (the assemblage mostly indicating the CNO3-CNO4/CNO5 biozones) mudstone/shale clasts, and four Serravallian (CNM10) mudstone clasts, with the rest of the analyzed sediments being assigned to the biozones CNM6–7, CNM7, and CNM8–9. Previous studies have dated analogous sediments from the broader Olimpi/Prometheus 2 area as Burdigalian–Langhian and early Serravallian. Almost all examined samples included Miocene, Oligocene, Eocene, and Cretaceous reworked nannofossils.

Both clasts and matrices of the cored mud breccias were subjected to Rock-Eval pyrolysis in order to evaluate the sediments' source rock potential for hydrocarbon generation. For this evaluation, the total organic carbon (TOC) values, kerogen type, and thermal maturation were determined. The results showed (i) the distribution of the majority of the data points associated with the pyrolyzed sediments close to the type III kerogen curve, (ii) organic-rich (TOC >0.5%) and organic-poor sediments (TOC <0.5%), and (iii) "immature" (Tmax <434 °C) to nearly "mature" (Tmax of 430–434 °C) material.

On the other hand, the pyrolysis results remarkably revealed one CNM10 mudstone clast from the Gelendzhik MV plateau with a high TOC content (~2%) and composed of organic matter of a mixed type II/III kerogen (oil prone). In addition, the high hydrogen index and relatively low oxygen index of the previous clast together with its enhanced calcareous and siliceous microfossil content provide good evidence that the source of this material is a sapropelic rock.

Finally, we believe that the data provided by the current investigation can be significant for the oil and gas exploration of the wider study area (offshore southern Crete), since they shed light on the occurrence and stratigraphic position of hydrocarbon source rocks, although they are estimated to be below the thermal condition for oil generation. Because the Mediterranean Ridge accretionary complex is a highly-tectonized region, it is reasonable to assume that the lateral extension of the determined Miocene source rocks

might potentially occur deeper in the stratigraphic column of the broader Olimpi mud volcano area, thus reaching the oil/gas window maturities.

Author Contributions: Conceptualization, A.N., M.V.T. and A.G.; methodology, M.V.T., G.R., N.P., A.G., I.H. and A.N.; validation, M.V.T., A.N., I.P., G.R., N.P., I.H. and A.G.; investigation, M.V.T., A.N., I.P., G.R. and A.G.; data curation, A.N., M.V.T., N.P. and I.P.; writing—original draft preparation, A.N., M.V.T., I.P., G.R. and A.G.; writing—review and editing, A.N., M.V.T., I.P. and N.P.; visualization, A.N., M.V.T., I.P., N.P. and G.R.; supervision, M.V.T., A.G. and G.R. All authors have read and agreed to the published version of the manuscript.

Funding: This research was funded by the General Secretariat for Research and Technology of Greece within the framework of the Programming Agreements with the Hellenic Research Centers for the period 2014–2016.

Institutional Review Board Statement: Not applicable.

Informed Consent Statement: Not applicable.

Data Availability Statement: The data presented in this study are available in Appendix A.

Acknowledgments: The technical support provided by the captain and crew of the R/V Aegaeo is highly acknowledged. This work has been accomplished in the framework of the Interdisciplinary Postgraduate Study Program "Palaeontology-Geobiology".

Conflicts of Interest: The authors declare no conflict of interest.

Appendix A

The information derived from the macroscopic examination and biostratigraphic and geochemical analyses of the collected mud breccia samples is presented in the Tables A1–A5 provided below. This information includes:

- Sampling intervals and sample types (matrix or clast);
- Percentages of nannofossils in the images captured by the Leica DMLSP optical polarizing light microscope, dating of sediments and rock types;
- Macroscopic observations such as consolidation degree of samples, sediment color, fissility occurrence, and characteristic sound during samples' homogenization that is indicative of quartz presence;
- Parameters measured during each Rock-Eval pyrolysis run such as S1, S2, and S3 peaks;
- Parameters calculated from the Rock-Eval experimental data such as Tmax, HI, and OI, and TOC, MinC, and carbonate contents.

The consolidation degree of the matrix intervals has already been described by Panagiotopoulos et al. [26]. The consolidation degree of the investigated clasts was determined using an empirical method, following the criteria described below:

- Soft: the rock can be broken between fingers;
- Soft to semi-consolidated: the rock can be broken between fingers and a hard object (e.g., mortar or table surface) with normal effort;
- Semi-consolidated: the rock can be broken between fingers and a hard object (e.g., mortar or table surface) with a lot of effort;
- Semi- to well-consolidated: the rock can be broken between pestle and mortar with normal effort;
- Well-consolidated: the rock can be broken between pestle and mortar with a lot of effort.

All nannofossil assemblages identified during the present study together with their semi-quantitative determination are displayed in the Tables A6–A47 provided below. Note that the counted specimens are expressed vs. the number of fields of view (see Section 2.2 for details).

Finally, Figure A1 illustrates representative Rock-Eval pyrograms showing typical unimodal and almost symmetric S2 curves.

Table A1. Gelendzhik MV (LEV1GC core).

Core Interval (cm)	Samp. Type	Nannofossils (%)	Dating	Rock Type	Consolid. Degree	Color	Remark	OI mg g^{-1}	HI mg g^{-1}	Tmax °C	TOC %	MinC %	S1 mg g^{-1}	S2 mg g^{-1}	S3 mg g^{-1}	Carbonate %
4–6	matrix	30	mixed; mostly Oligocene–Miocene	sandy mud	soft	greenish grey (10GY5/1)	quartz sound	228.09	39.33	421	0.89	1.85	0.01	0.35	2.03	14.76
4–6	clast 1	70–80	CNM10	mudstone	soft	pale yellow (5Y8/3)		91.09	437.62	413	2.02	4.66	0.39	8.84	1.84	37.17
4–6	clast 2	10	CNM10	mudstone	semi-well	very dark grey (N3/)		331.15	114.75	?	0.61	0.35	0.01	0.7	2.02	2.79
18–20	matrix	30	mixed; mostly Oligocene–Miocene	sandy mud	firm	greenish grey (10GY5/1)	quartz sound	366.04	58.49	426	0.53	1.24	0.01	0.31	1.94	9.89
18–20	clast 1	50	CNM8–9	mudstone	semi	greenish grey (5GY6/1)		95.38	155.38	?	0.65	0.36	0	1.01	0.62	2.87
65–67	matrix	30	mixed; mostly Oligocene–Miocene	sandy mud	firm	dark greenish grey (10GY4/1)		431.91	87.23	?	0.47	1.01	0.02	0.41	2.03	8.06
65–67	clast 1	<10	CNM10	mudstone	semi	grey (N5/)		354	116	?	0.5	0.8	0.02	0.58	1.77	6.38

Table A2. Heraklion MV (LEV3GC core).

Core Interval (cm)	Samp. Type	Nannofossils (%)	Dating	Rock Type	Consolid. Degree	Color	Remark	OI mg g^{-1}	HI mg g^{-1}	Tmax °C	TOC %	MinC %	S1 mg g^{-1}	S2 mg g^{-1}	S3 mg g^{-1}	Carbonate %
2–5	matrix	almost barren	undetermined	sandy mud	very soft	dark greenish grey (10GY4/1)	quartz sound	32	200	?	0.25	0.06	0	0.5	0.08	0.48
25–27	matrix	30	mixed; mostly Oligocene–Miocene	sandy mud	very stiff	greenish grey (7.5GY5/1)	quartz sound	138.3	34.04	418	0.94	2.8	0.01	0.32	1.3	22.33
65–67	clast 1	30–40	CNM6–7	mudstone	soft	pale yellow (5Y8/3)		126.8	131.96	434	0.97	5.04	0.01	1.28	1.23	40.2
65–67	clast 2	?	undetermined	mudstone	soft	light grey (N7/)		142.67	41.33	416	0.75	4.59	0	0.31	1.07	36.61

Table A3. Moscow MV (LEV5GC core).

Core Interval (cm)	Samp. Type	Nannofossils (%)	Dating	Rock Type	Consolid. Degree	Color	Remark	OI mg g^{-1}	HI mg g^{-1}	Tmax °C	TOC %	MinC %	S1 mg g^{-1}	S2 mg g^{-1}	S3 mg g^{-1}	Carbonate %
10–12	matrix	30	mixed; mostly Oligocene–Miocene	sandy mud	very stiff	greenish grey (7.5GY5/1)	quartz sound	529.41	35.29	426	0.34	2.68	0	0.12	1.8	21.38
10–12	clast 1	~10	mainly CNO3-CNO4/CNO5	shale	semi	greenish grey (5GY6/1)	sub-parallel fissility	516.67	58.33	419	0.36	2.46	0	0.21	1.86	19.62
10–12	clast 2	~30	mixed; mostly Oligocene–Miocene	mudstone	semi	dark grey (N4/)		481.82	145.45	?	0.11	0.18	0.01	0.16	0.53	1.44
40–42	clast 1	70–80	CNO4/CNO5	mudstone	soft-semi	pale yellow (5Y8/3)		465.79	21.05	427	0.38	6.04	0	0.08	1.77	48.18
40–42	clast 2	~10	mixed; mostly Oligocene–Miocene	mudstone	semi-well	very dark grey (N3/)		373.68	100	?	0.19	0.26	0	0.19	0.71	2.07
70–72	clast 1	30–40	CNM6–7	carbonate mudstone	semi	grey (N6/)		230.59	220	433	0.85	6.71	0.02	1.87	1.96	53.52
100–102	matrix	30	mixed; mostly Oligocene–Miocene	sandy mud	very stiff	greenish grey (10GY5/1)	quartz sound	490.91	57.58	424	0.33	1.93	0	0.19	1.62	15.39
100–102	clast 1	≤10	mainly CNO3-CNO4/CNO5	mudstone	semi	dark grey (N4/)		287.5	64.58	426	0.48	0.43	0	0.31	1.38	3.43
100–102	clast 2	20–30	CNM10	mudstone	semi-well	grey (N6/)		195.83	91.67	423	0.24	1.16	0	0.22	0.47	9.25
123–125	matrix	30	mixed; mostly Oligocene–Miocene	sandy mud	very stiff	greenish grey (10GY5/1)	quartz sound	497.14	68.57	427	0.35	1.93	0.01	0.24	1.74	15.39
123–125	clast 1	almost barren	undetermined	mudstone	semi	dark greyish brown (10YR4/2)		249.12	61.4	?	0.57	0.22	0.02	0.35	1.42	1.75
123–125	clast 2	30	CNM7	carbonate mudstone	semi-well	pale yellow (5Y8/3)		539.13	17.39	?	0.23	8.23	0.01	0.04	1.24	65.64

Table A4. Milano MV (LEV7GC core).

Core Interval (cm)	Samp. Type	Nannofossils (%)	Dating	Rock Type	Consolid. Degree	Color	Remark	OI mg g^{-1}	HI mg g^{-1}	Tmax °C	TOC %	MinC %	S1 mg g^{-1}	S2 mg g^{-1}	S3 mg g^{-1}	Carbonate %
12–14	matrix	30	mixed; mostly Oligocene–Miocene	sandy mud	very soft	greenish grey (10GY5/1)	quartz sound	473.17	58.54	427	0.41	1.64	0.01	0.24	1.94	13.08
40–43	matrix	30	mixed; mostly Oligocene–Miocene	sandy mud	very soft	greenish grey (10GY5/1)	quartz sound	446.94	67.35	427	0.49	1.67	0.01	0.33	1.94	13.32
40–43	clast 1	<10	CNM8–9	shale	well	dark greyish brown (10YR4/2)	parallel fissility	270.49	88.52	?	0.61	0.4	0.01	0.54	1.65	3.19
40–43	clast 2	20–30	CNM8–9	mudstone	semi	greenish grey (5GY6/1)		554.17	37.5	399	0.48	2.29	0.01	0.18	2.66	18.27
78–80	matrix	30	mixed; mostly Oligocene–Miocene	sandy mud	soft	dark greenish grey (10GY4/1)	quartz sound	380.43	65.22	432	0.46	1.72	0.01	0.3	1.75	13.72
78–80	clast 1	<5	CNM8–9	mudstone	semi-well	dark grey (N4/1)		265.71	42.86	427	0.35	1.46	0	0.15	0.93	11.64
78–80	clast 2	almost barren	undetermined	mudstone	semi	greenish grey (5GY6/1)		477.27	52.27	413	0.44	0.62	0.01	0.23	2.1	4.95

Table A5. Leipzig MV (LEV9GC core).

Core Interval (cm)	Samp. Type	Nannofossils (%)	Dating	Rock Type	Consolid. Degree	Color	Remark	OI mg g^{-1}	HI mg g^{-1}	Tmax °C	TOC %	MinC %	S1 mg g^{-1}	S2 mg g^{-1}	S3 mg g^{-1}	Carbonate %
10–13	matrix	30	mixed; mostly Oligocene–Miocene	sandy mud	very soft	greenish grey (10GY5/1)	quartz sound	224.62	52.31	428	0.65	1.52	0.01	0.34	1.46	12.12
10–13	clast 1	≤10	CNM8–9	mudstone	well	very dark grey (N3/)		189.93	93.22	427	0.59	0.61	0.01	0.55	1.12	4.87
67–69	clast 1	<10	CNM6–7	mudstone	soft	grey (N/6)		76.12	76.12	434	0.67	0.37	0.01	0.51	0.51	2.95
67–69	clast 2	almost barren	undetermined	sandstone	semi-well	greyish green (5G5/2)		200	100	?	0.03	0.03	0	0.03	0.06	0.24
98–100	matrix	30	mixed; mostly Oligocene–Miocene	sandy mud	very stiff	dark greenish grey (10GY4/1)	quartz sound	168.75	56.25	427	0.48	1.58	0	0.27	0.81	12.6
98–100	clast 1	~10	mixed; mostly Oligocene–Miocene	carbonate mudstone/ sandstone	semi-well	light grey (N7/)/dark grey (N4/)	interbedding, quartz sound	207.69	42.31	424	0.26	9.35	0	0.11	0.54	74.58
98–100	clast 2	30–40	CNM6–7	mudstone	semi-well	grey (N/6)		127.59	63.22	424	0.87	3.58	0	0.55	1.11	28.55
98–100	clast 3	50–60	CNM8–9	shale	well	Grey (N/6)	sub-parallel fissility	291.67	94.44	423	0.36	6.09	0	0.34	1.05	48.57
128–130	matrix	30	mixed; mostly Oligocene–Miocene	sandy mud	very stiff	dark greenish grey (10GY4/1)	quartz sound	155.1	61.22	422	0.49	1.63	0	0.3	0.76	13
128–130	clast 1	?	undetermined	shale	semi-well	reddish brown (2.5YR4/4)	sub-parallel fissility	321.62	51.35	427	0.37	0.93	0	0.19	1.19	7.42
128–130	clast 2	20–30	CNM7	carbonate mudstone	semi	pale yellow (5Y8/3)		220	130	428	0.4	7.23	0	0.52	0.88	57.67
128–130	clast 3	~5	CNM8–9	mudstone	semi	light grey (N7/)		73.33	64	426	0.75	0.26	0	0.48	0.55	2.07

Table A6. Gelendzhik MV.

LEV1GC 4–6 Matrix					
Mixed; Mostly Oligocene–Miocene					
Species	A	C	F	R	Specimens Counted
Neogene					
Calcidiscus leptoporus		X			7
Calcidiscus macintyrei		X			7
Discoaster quinqueramus				X	1
Discoaster variabilis			X		4
Helicosphaera carteri			X		6
Reticulofenestra pseudoumbilicus		X			9
Umbilicosphaera jafari				X	1
Umbilicosphaera rotula		X			7
Sphenolithus disbelemnos				X	1
Sphenolithus tintinnabulum				X	1
Sphenolithus neoabies			X		5
Paleogene					
Micrantholithus sp.				X	1
Reticulofenestra bisecta		X			9
Long-range Paleogene–Neogene					
Coccolithus pelagicus	X				24
Coronocyclus mesostenos				X	2
Cyclicargolithus floridanus	X				20
Discoaster sp.		X			8
Pontosphaera multipora				X	1
Rhabdosphaera sp.				X	3
small reticulofenestroids	X				29
Sphenolithus moriformis			X		6
Helicosphaera mediterranea				X	2
Helicosphaera sp.			X		6
Sphenolithus sp.				X	3
Other					
Siliceous microfossils				X	2

Table A7. Gelendzhik MV.

LEV1GC 4–6 Clast 1					
Biozone: CNM10					
Species	A	C	F	R	Specimens Counted
Neogene					

Calcidiscus leptoporus	X				30
Calcidiscus macintyrei				X	1
Discoaster formosus				X	3
Discoaster braarudii				X	3
Discoaster kugleri				X	2
Discoaster variabilis				X	3
Helicosphaera carteri				X	2
Umbilicosphaera rotula				X	2
Long-range Paleogene–Neogene					
Coccolithus pelagicus				X	3
Discoaster sp.	X				13
small reticulofenestroids	X				10
Sphenolithus moriformis				X	1
Other					
Siliceous microfossils	X				20

Table A8. Gelendzhik MV.

LEV1GC 4–6 Clast 2					
Biozone: CNM10					
Species	A	C	F	R	Specimens Counted
Neogene					
Calcidiscus leptoporus				X	1
Calcidiscus macintyrei				X	2
Coccolithus miopelagicus				X	2
Discoaster apetalus				X	1
Discoaster assymetricus				X	1
Discoaster exilis				X	1
Discoaster kugleri				X	2
Discoaster ulnatus				X	1
Discoaster variabilis		X			8
Helicosphaera carteri			X		5
Reticulofenestra pseudoumbilicus	X				32
Sphenolithus disbelemnos				X	1
Sphenolithus				X	2

dissimilis					
Umbilicosphaera foliosa			X		5
Umbilicosphaera rotula				X	1
Paleogene					
Reticulofenestra bisecta	X				10
Reticulofenestra hillae				X	1
Sphenolithus predistentus				X	1
Long-range Paleogene–Neogene					
Coccolithus pelagicus	X				21
Coronocyclus nitscens				X	1
Cyclicargolithus floridanus				X	3
Discoaster deflandrei				X	1
Discoaster sp.	X				23
Pontosphaera multipora				X	3
Reticulofenestra perplexa				X	2
small reticulofenestroids	X				16
Sphenolithus moriformis	X				11

Table A9. Gelendzhik MV.

LEV1GC 18–20 Matrix					
Mixed; Mostly Oligocene–Miocene					
Species	A	C	F	R	Specimens Counted
Neogene					
Calcidiscus leptoporus			X		5
Calcidiscus macintyrei				X	3
Discoaster apetalus				X	1
Discoaster calcaris				X	1
Discoaster variabilis			X		6
Gephyrocapsa <3 μm				X	1
Helicosphaera carteri		X			9
Helicosphaera selli				X	1
Reticulofenestra	X				10

pseudoumbilicus					
Sphenolithus abies				X	1
Sphenolithus heteromorphus				X	1
Umbilicosphaera foliosa				X	2
Umbilicosphaera jafari				X	2
Paleogene					
Cyclicargolithus abisectus				X	1
Discoaster saipanensis				X	1
Discoaster spinescens				X	1
Micrantholithus sp.				X	1
Reticulofenestra hillae				X	1
Reticulofenestra bisecta			X		5
Long-range Paleogene–Neogene					
Coccolithus pelagicus	X				29
Coronocyclus nitescens				X	1
Cyclicargolithus floridanus	X				28
Discoaster sp.	X				18
Pontosphaera multipora				X	1
Pontosphaera sp.				X	3
Rhabdosphaera sp.				X	1
small reticulofenestroids	X				19
Sphenolithus moriformis				X	3

Table A10. Gelendzhik MV.

LEV1GC 18–20 Clast 1					
Biozone: CNM8–9					
Species	A	C	F	R	Specimens Counted
Neogene					
Calcidiscus leptoporus			X		4
Calcidiscus macintyrei	X				12
Discoaster variabilis			X		5

Helicosphaera carteri		X		5
Helicosphaera walbersdorfensis		X		5
Reticulofenestra pseudoumbilicus	X			13
Sphenolithus abies		X		4
Sphenolithus heteromorphus			X	1
Umbilicosphaera rotula		X		4
Paleogene				
Calcidiscus gerrardii			X	1
Micrantholithus sp.			X	1
Reticulofenestra hillae			X	1
Reticulofenestra reticulata			X	1
Reticulofenestra bisecta			X	2
Zygrhablithus bijugatus			X	1
Long-range Paleogene–Neogene				
Braarudosphaera bigelowii		X		4
Coccolithus pelagicus	X			22
Coronocyclus nitescens			X	1
Cyclicargolithus floridanus			X	1
Discoaster sp.		X		7
Helicosphaera intermedia			X	1
Helicosphaera mediterranea			X	1
Pontosphaera multipora			X	2
Pontosphaera sp.			X	3
Reticulofenestra perplexa	X			20
Rhabdosphaera sp.			X	2
small reticulofenestroids	X			25
Sphenolithus moriformis		X		6
Cretaceous				
Zeugrhabdotus sp.			X	1

Table A11. Gelendzhik MV.

LEV1GC 65–67 Matrix					
Mixed; Mostly Oligocene–Miocene					
Species	A	C	F	R	Specimens Counted
Neogene					
Calcidiscus leptoporus				X	2
Calcidiscus macintyrei				X	3
Discoaster braarudii				X	2
Discoaster cauliflorus				X	1
Discoaster decorus				X	2
Discoaster exilis				X	3
Discoaster variabilis		X			9
Helicosphaera carteri		X			9
Helicosphaera walbersdorfensis				X	1
Helicosphaera wallichi				X	3
Reticulofenestra pseudoumbilicus	X				17
Sphenolithus heteromorphus				X	1
Umbilicosphaera jafari			X		6
Umbilicosphaera rotula				X	2
Helicosphaera etholonga				X	1
Paleogene					
Discoaster barbadiensis				X	1
Reticulofenestra hillae				X	2
Reticulofenestra bisecta			X		5
Long-range Paleogene–Neogene					
Coccolithus pelagicus	X				13
Coronocyclus mesostenos		X			8
Cyclicargolithus floridanus	X				11
Discoaster sp.			X		6
Pontosphaera discopora				X	1

Pontosphaera multipora		X			8
Pontosphaera sp.				X	1
Reticulofenestra perplexa				X	3
Rhabdosphaera sp.				X	2
small reticulofenestroids	X				13
Sphenolithus moriformis		X			9

Table A12. Gelendzhik MV.

LEV1GC 65–67 Clast 1					
Biozone: CNM10					
Species	A	C	F	R	Specimens Counted
Neogene					
Calcidiscus macintyrei				X	4
Discoaster braarudii				X	4
Discoaster decorus				X	2
Discoaster kugleri				X	1
Discoaster variabilis			X		4
Gephyrocapsa <3 μm				X	1
Helicosphaera carteri	X				10
Helicosphaera dissimilis				X	1
Helicosphaera selli				X	1
Reticulofenestra pseudoumbilicus	X				22
Sphenolithus delphix				X	1
Sphenolithus heteromorphus				X	1
Sphenolithus neoabies				X	1
Umbilicosphaera jafari				X	2
Umbilicosphaera rotula				X	2
Paleogene					
Discoaster barbadiensis					
Helicosphaera recta				X	1
Reticulofenestra hillae				X	3
Reticulofenestra bisecta				X	3
Long-range Paleogene–Neogen					

e					
Coccolithus pelagicus	X				16
Coronocyclus mesostenos				X	3
Cyclicargolithus floridanus			X		5
Discoaster deflandrei				X	1
Pontosphaera multipora				X	2
Pontosphaera sp.				X	3
Reticulofenestra perplexa				X	2
Rhabdosphaera sp.				X	2
small reticulofenestroids	X				32
Sphenolithus moriformis				X	1

Table A13. Heraklion MV.

LEV3GC 2–5 Matrix
Biozone: undetermined

Table A14. Heraklion MV.

LEV3GC 25–27 Matrix					
Mixed; Mostly Oligocene–Miocene					
Species	A	C	F	R	Specimens Counted
Neogene					
Calcidiscus leptoporus			X		4
Coccolithus miopelagicus			X		4
Discoaster variabilis				X	2
Helicosphaera carteri			X		3
Reticulofenestra pseudoumbilicus			X		4
Sphenolithus abies				X	1
Sphenolithus cometa				X	3
Sphenolithus heteromorphus	X				10
Umbilicosphaera rotula				X	1
Paleogene					
Reticulofenestra bisecta				X	2
Reticulofenestra lockeri				X	2

Sphenolithus predistentus				X	1
Long-range Paleogene–Neogene					
Coronocyclus mesostenos				X	1
Discoaster sp.				X	2
Sphenolithus truaxii				X	2
Helicosphaera sp.		X			8
small reticulofenestroids	X				10
Reticulofenestra perplexa	X				11
Sphenolithus moriformis	X				11
Cyclicargolithus floridanus	X				21
Coccolithus pelagicus	X				34
Cretaceous					
undetermined Cretaceous sp.				X	1

Table A15. Heraklion MV.

LEV3GC 65–67 Clast 1					
Biozone: CNM6–7					
Species	A	C	F	R	Specimens Counted
Neogene					
Calcidiscus leptoporus				X	2
Calcidiscus macintyrei				X	3
Calcidiscus premacintyrei				X	1
Discoaster variabilis		X			8
Gephyrocapsa <3 μm				X	1
Helicosphaera ampliamperta		X			5
Helicosphaera carteri	X				16
Helicosphaera walbersdorfensis				X	6
Sphenolithus dissimilis				X	2
Sphenolithus heteromorphus		X			5
Umbilicosphaera foliosa				X	1
Umbilicosphaera		X			9

jafari					
Umbilicosphaera rotula		X			6
Paleogene					
Discoaster barbadiensis				X	1
Reticulofenestra lockeri				X	1
Reticulofenestra bisecta				X	2
Sphenolithus predistentus				X	2
Long-range Paleogene–Neogene					
Coccolithus pelagicus	X				61
Coronocyclus mesostenos				X	1
Cyclicargolithus floridanus	X				15
Discoaster deflandrei		X			12
Discoaster sp.	X				35
Helicosphaera intermedia		X			7
Pontosphaera sp.				X	2
small reticulofenestroids	X				25
Sphenolithus moriformis	X				13
Cretaceous					
undetermined Cretaceous sp.				X	1
Eiffellithus turriseiffelii				X	1

Table A16. Heraklion MV.

LEV3GC 65–67 Clast 2
Biozone: undetermined

Table A17. Moscow MV.

LEV5GC 10–12 Matrix					
Mixed; Mostly Oligocene–Miocene					
Species	A	C	F	R	Specimens Counted
Neogene					
Calcidiscus macintyrei			X		4

Calcidiscus premacintyrei			X	1
Coccolithus miopelagicus			X	1
Discoaster variabilis			X	1
Gephyrocapsa <3 μm			X	2
Helicosphaera carteri			X	3
Helicosphaera orientalis			X	2
Pseudoemiliania lacunosa			X	2
Reticulofenestra pseudoumbilicus	X			9
Sphenolithus heteromorphus			X	2
Syracosphaera pulchra			X	1
Umbilicosphaera jafari		X		4
Umbilicosphaera rotula			X	1
Paleogene				
Chiasmolithus sp.			X	1
Coccolithus formosus			X	3
Cyclicargolithus abisectus			X	3
Discoaster barbadiensis			X	1
Discoaster multiradiatus			X	1
Helicosphaera recta			X	1
Reticulofenestra lockeri			X	1
Reticulofenestra hillae			X	1
Reticulofenestra stavensis			X	1
Sphenolithus ciperoensis			X	1
Sphenolithus distentus			X	1
Zygrhablithus bijugatus			X	1
Long-range Paleogene–Neogene				
Coccolithus pelagicus	X			11
Coronocyclus mesostenos			X	3
Cyclicargolithus		X		5

floridanus					
Discoaster deflandrei				X	1
Discoaster sp.			X		5
Helicosphaera intermedia				X	1
Pontosphaera multipora				X	1
Pontosphaera sp.				X	2
Reticulofenestra perplexa			X		4
small reticulofenestroids				X	3
Sphenolithus moriformis			X		4
Cretaceous					
undetermined Cretaceous sp.				X	1

Table A18. Moscow MV.

LEV5GC 10–12 Clast 1					
Mainly CNO3-CNO4/CNO 5					
Species	A	C	F	R	Specimens Counted
Neogene					
Coccolithus miopelagicus				X	1
Discoaster discissus				X	1
Discoaster durioi				X	1
Discoaster exiis				X	3
Gephyrocapsa <3 μm				X	1
Helicosphaera carteri			X		4
Sphenolithus abies				X	3
Paleogene					
Coccolithus formosus				X	3
Discoaster barbadiensis				X	1
Discoaster multiradiatus				X	1
Discoaster nodifer				X	1
Helicosphaera compacta				X	2
Helicosphaera recta				X	2
Reticulofenestra lockeri		X			7
Reticulofenestra bisecta			X		4
Reticulofenestra				X	2

reticulata					
Sphenolithus distentus		X			8
Sphenolithus obtusus				X	1
Sphenolithus peartiae				X	1
Sphenolithus predistentus				X	2
Zygrhablithus bijugatus			X		4
Long-range Paleogene–Neogene					
Coccolithus pelagicus		X			10
Coronocyclus mesostenos				X	1
Cyclicargolithus floridanus	X				71
Discoaster deflandrei		X			9
Discoaster leroyi				X	1
Discoaster sp.		X			8
Helicosphaera intermedia				X	1
Helicosphaera mediterranea				X	3
Pontosphaera multipora				X	3
Pontosphaera sp.				X	1
Sphenolithus moriformis			X		7
small reticulofenestroids		X			11
Cretaceous					
Arkhangelskiales sp.				X	3
Broinsonia parca				X	1
undetermined Cretaceous sp.				X	3
Diazomatolithus lehmanii				X	1
Eiffelithus sp.				X	2
Zeugrhabdotus				X	2

Table A19. Moscow MV.

LEV5GC 10–12 Clast 2					
Mixed; Mostly Oligocene–Miocene					
Species	A	C	F	R	Specimens Counted
Neogene					
Calcidiscus			X		5

leptoporus				
Calcidiscus macintyrei		X		5
Coccolithus miopelagicus			X	1
Discoaster kugleri			X	1
Discoaster variabilis			X	1
Discoater durioi			X	1
Gephyrocapsa <3 μm			X	3
Helicosphaera carteri	X			6
Helicosphaera orientalis			X	1
Helicosphaera selli			X	1
Helicosphaera stalis			X	2
Pontosphaera japonica			X	1
Pseudoemiliania lacunosa			X	2
Reticulofenestra pseudoumbilicus	X			7
Rhabdosphaera? sp.		X		3
Sphenolithus abies		X		3
Sphenolithus belemnos			X	1
Sphenolithus dissimilis			X	1
Sphenolithus heteromorphus	X			6
Syracosphaera pulchra			X	1
Umbilicosphaera foliosa			X	3
Umbilicosphaera jafari	X			7
Umbilicosphaera rotula			X	1
Umbilicosphaera sibogae			X	1
Paleogene				
Coccolithus formosus			X	2
Cyclicargolithus abisectus		X		5
Discoaster multiradiatus			X	1
Helicosphaera compacta			X	2
Reticulofenestra lockeri		X		4
Reticulofenestra bisecta	X			9

Reticulofenestra hillae				X	1
Sphenolithus capricornatus				X	1
Sphenolithus ciperoensis				X	2
Sphenolithus distentus				X	3
Sphenolithus predistentus				X	1
Sphenolithus umbrellus				X	2
Zygrhablithus bijugatus				X	1
Long-range Paleogene–Neogene					
Coccolithus pelagicus	X				15
Coronocyclus mesostenos			X		6
Coronocyclus nitescens				X	1
Cyclicargolithus floridanus	X				26
Discoaster deflandrei			X		5
Discoaster salomoni				X	2
Discoaster sp.				X	3
Helicosphaera intermedia			X		5
Helicosphaera mediterranea			X		3
Helicosphaera sp.				X	1
Pontosphaera multipora				X	1
Pontosphaera sp.				X	2
Sphenolithus moriformis				X	3
small reticulofenestroids	X				26

Table A20. Moscow MV.

LEV5GC 40–42 Clast 1					
Biozone: CNO4/CNO5					
Species	A	C	F	R	Specimens Counted
Paleogene					
Coccolithus eopelagicus				X	2

Cyclicargolithus abisectus				X	2
Discoaster barbadiensis				X	1
Helicosphaera obliqua				X	1
Helicosphaera recta				X	2
Reticulofenestra lockeri				X	1
Reticulofenestra bisecta			X		5
Sphenolithus ciperoensis			X		4
Sphenolithus distentus				X	2
Sphenolithus predistentus				X	1
Zygrhablithus bijugatus			X		6
Long-range Paleogene–Neogene					
Braarudosphaera bigelowi				X	1
Coccolithus pelagicus	X				29
Coronocyclus mesostenos			X		5
Coronocyclus nitescens				X	3
Cyclicargolithus floridanus	X				81
Discoaster deflandrei		X			11
Discoaster sp.			X		3
Helicosphaera euphratis				X	2
Helicosphaera intermedia				X	3
Helicosphaera leesiae				X	2
Helicosphaera mediterranea				X	2
Pontosphaera japonica			X		6
Rhabdosphaera? sp.			X		4
Sphenolithus conicus			X		4
Sphenolithus moriformis	X				20
Cretaceous					
Broinsonia parca				X	1
Eiffelithus sp.				X	1
Rhagodiscus				X	1

infinitus					

Table A21. Moscow MV.

LEV5GC 40–42 Clast 2					
Mixed; Mostly Oligocene–Miocene					
Species	A	C	F	R	Specimens Counted
Neogene					
Calcidiscus macintyrei				X	3
Coccolithus miopelagicus				X	1
Helicosphaera carteri			X		4
Helicosphaera princei				X	1
Helicosphaera stalis				X	1
Reticulofenestra pseudoumbilicus				X	2
Rhabdosphaera? sp.				X	2
Sphenolithus dissimilis				X	1
Sphenolithus heteromorphus				X	2
Sphenolithus tintinnabulum				X	1
Umbilicosphaera jafari			X		5
Umbilicosphaera rotula				X	3
Paleogene					
Calcidiscus gerrardii				X	1
Coccolithus crassus?				X	1
Coccolithus formosus			X		7
Cyclicargolithus abisectus				X	2
Cyclicargolithus parvus				X	1
Discoaster wemmelensis				X	1
Helicosphaera leesiae				X	1
Helicosphaera recta				X	1
Reticulofenestra daviesii				X	1
Reticulofenestra lockeri				X	1
Reticulofenestra bisecta			X		5
Sphenolithus ciperoensis				X	3

Sphenolithus distentus				X	2
Sphenolithus umbrellus				X	1
Zygrhablithus bijugatus				X	1
Long-range Paleogene–Neogene					
Coccolithus pelagicus	X				17
Coronocyclus mesostenos				X	3
Cyclicargolithus floridanus	X				33
Discoaster deflandrei				X	3
Discoaster sp.				X	1
Pontosphaera sp.				X	1
small reticulofenestroids	X				17
Sphenolithus moriformis			X		4

Table A22. Moscow MV.

LEV5GC 70–72 Clast 1					
Biozone: CNM6–7					
Species	A	C	F	R	Specimens Counted
Neogene					
Calcidiscus macintyrei				X	1
Calcidiscus premacintyrei				X	3
Discoaster exilis				X	1
Helicosphaera ampliaperta			X		6
Helicosphaera carteri			X		5
Sphenolithus cometa				X	1
Sphenolithus dibelemnos				X	1
Sphenolithus heteromorphus			X		5
Umbilicosphaera jafari			X		4
Paleogene					
Cyclicargolithus abisetus				X	2
Discoaster barbadiensis				X	1
Reticulofenestra				X	1

lockeri					
Long-range Paleogene–Neogene					
Coccolithus pelagicus	X				12
Coronocyclus mesostenos				X	4
Cyclicargolithus floridanus	X				19
Discoaster deflandrei			X		5
Discoaster sp.				X	8
Helicosphaera intermedia				X	4
Pontosphaera multipora				X	2
Pontosphaera sp.				X	1
Reticulofenestra perplexa				X	4
small reticulofenestroids	X				9
Sphenolithus moriformis	X				15
Cretaceous					
Dizomatolithus lehmanii			X		1

Table A23. Moscow MV.

LEV5GC 100–102 Matrix					
Mixed; Mostly Oligocene–Miocene					
Species	A	C	F	R	Specimens Counted
Neogene					
Calcidiscus leptoporus				X	4
Calcidiscus macintyrei				X	3
Discoaster exilis				X	2
Gephyrocapsa <3 μm					1
Helicosphaera carteri				X	4
Reticulofenestra pseudoumbilicus	X				18
Schyphosphaera intermedia				X	1
Sphenolithus cometa				X	2
Sphenolithus heteromorphus				X	4
Umbilicosphaera jafari				X	2

Umbilicosphaera rotula				X	2
Paleogene					
Discoaster multiradiatus				X	1
Discoaster nodifer				X	1
Sphenolithus ciperoensis				X	2
Sphenolithus distentus				X	1
Sphenolithus predistentus				X	2
Zygrhablithus bijugatus				X	2
Long-range Paleogene–Neogene					
Coccolithus pelagicus	X				18
Coronocyclus mesostenos				X	2
Cyclicargolithus floridanus	X				17
Discoaster deflandrei				X	3
Discoaster sp.			X		5
Sphenolithus moriformis			X		6
Cretaceous					
Diazomatolithus lehmanii				X	1

Table A24. Moscow MV.

LEV5GC 100–102 Clast 1					
Mainly CNO3-CNO4/CNO 5					
Species	A	C	F	R	Specimens Counted
Neogene					
Coccolithus miopelagicus				X	1
Discoaster kugleri				X	2
Reticulofenestra pseudoumbilicus				X	3
Umbilicosphaera jafari				X	3
Paleogene					
Coccolithus formosus		X			8
Reticulofenestra lockeri				X	2

Reticulofenestra reticulata				X	1
Reticulofenestra stavensis			X		5
Sphenolithus distentus		X			8
Sphenolithus peartiae				X	3
Umbilicosphaera detecta				X	1
Zygrhablithus bijugatus				X	1
Long-range Paleogene–Neogene					
Coccolithus pelagicus	X				22
Coronocyclus nitescens				X	2
Cyclicargolithus floridanus	X				66
Discoaster deflandrei				X	2
Helicosphaera euphratis				X	1
Helicosphaera intermedia				X	3
Helicosphaera leesiae				X	1
Helicosphaera sp.				X	1
Pontosphaera multipora				X	1
small reticulofenestroids	X				13
Sphenolithus moriformis	X				20
Cretaceous					
undetermined Cretaceous sp.				X	2
Zeugrhabdotus sp.				X	1

Table A25. Moscow MV.

LEV5GC 100–102 Clast 2					
Biozone: CNM10					
Species	A	C	F	R	Specimens Counted
Neogene					
Calcidiscus leptoporus				X	1
Calcidiscus macintyrei				X	2
Coccolithus miopelagicus				X	2

Discoaster kugleri				X	2
Discoaster variabilis				X	2
Gephyrocapsa <3 μm				X	2
Helicosphaera ampliaperta				X	3
Helicosphaera carteri		X			10
Pseudoemiliania lacunosa?				X	2
Reticulofenestra pseudoumbilicus	X				12
Sphenolithus heteromorphus			X		4
Umbilicosphaera foliosa				X	2
Umbilicosphaera jafari				X	2
Umbilicosphaera rotula				X	1
Paleogene					
Cyclicargolithus abisectus				X	2
Discoaster nodifer				X	1
Reticulofenestra lockeri				X	1
Reticulofenestra bisecta			X		4
Sphenolithus ciperoensis				X	1
Zygrhablithus bijugatus				X	1
Long-range Paleogene–Neogene					
Coccolithus pelagicus	X				38
Cyclicargolithus floridanus	X				36
Discoaster deflandrei				X	1
Discoaster sp.				X	1
Helicosphaera intermedia				X	2
Helicosphaera mediterranea				X	1
small reticulofenestroids	X				12
Sphenolithus moriformis	X				13
Cretaceous					
Diazomatolithus lehmanii				X	2
Eiffelithus sp.				X	1

other					
Siliceous microfossils				X	2

Table A26. Moscow MV.

LEV5GC 123–125 Matrix					
Mixed; Mostly Oligocene–Miocene					
Species	A	C	F	R	Specimens Counted
Neogene					
Calcidiscus leptoporus				X	2
Calcidiscus macintyrei				X	2
Discoaster kugleri				X	1
Gephyrocapsa <3 μm				X	2
Helicosphaera carteri			X		6
Reticulofenestra pseudoumbilicus		X			9
Sphenolithus heteromorphus				X	3
Umbilicosphaera jafari			X		4
Umbilicosphaera rotula				X	2
Paleogene					
Reticulofenestra bisecta				X	1
Sphenolithus ciperoensis				X	1
Sphenolithus distentus				X	2
Sphenolithus predistentus				X	1
Long-range Paleogene–Neogene					
Coccolithus pelagicus	X				16
Cyclicargolithus floridanus	X				11
Discoaster deflandrei				X	2
Discoaster sp.				X	2
Helicosphaera leesiae				X	1
Reticulofenestra perplexa			X		5
Sphenolithus moriformis		X			8
Sphenolithus sp.				X	1

Cretaceous					
undetermined Cretaceous sp.				X	1
Diazomatolithus lehmanii				X	2

Table A27. Moscow MV.

LEV5GC 123–125 Clast 1
Biozone: undetermined

Table A28. Moscow MV.

LEV5GC 123–125 Clast 2					
Biozone: CNM7					
Species	A	C	F	R	Specimens Counted
Neogene					
Coccolithus miopelagicus				X	2
Helicosphaera carteri		X			10
Sphenolithus heteromorphus	X				27
Paleogene					
Reticulofenestra bisecta				X	2
Long-range Paleogene–Neogene					
Coccolithus pelagicus	X				21
Cyclicargolithus floridanus	X				16
Discoaster deflandrei				X	1
Discoaster sp.			X		4
Helicosphaera intermedia				X	1
Micrantholithus sp.				X	1
Pontosphaera sp.			X		4
Reticulofenestra perplexa	X				30
small reticulofenestroids		X			10
Sphenolithus moriformis	X				15

Table A29. Milano MV.

LEV7GC 12–14 Matrix					
Mixed; Mostly Oligocene–Miocene					
Species	A	C	F	R	Specimens Counted
Neogene					
Calcidiscus leptoporus				X	1
Calcidiscus macintyrei			X		4
Coccolithus miopelagicus				X	1
Discoaster discissus				X	1
Discoaster durioi				X	1
Discoaster variabilis				X	1
Gephyrocapsa <3 μm				X	2
Helicosphaera carteri			X		4
Pseudoemiliania lacunosa				X	2
Reticulofenestra pseudoumbilicus	X				24
Sphenolithus heteromorphus				X	1
Umbilicosphaera jafari			X		2
Umbilicosphaera rotula				X	1
Paleogene					
Discoaster barbadiensis				X	3
Sphenolithus umbrellus				X	2
Long-range Paleogene–Neogene					
Braarudosphaera bigelowii				X	1
Coccolithus pelagicus	X				8
Cyclicargolithus floridanus	X				11
Discoaster deflandrei				X	3
Discoaster sp.				X	1
Helicosphaera intermedia				X	1
Pontosphaera multipora				X	2
Pontosphaera sp.				X	3

Reticulofenestra perplexa		X			6
small reticulofenestroids		X			10
Sphenolithus moriformis			X		3
Cretaceous					
Arkhangelskiella sp.				X	2
undetermined Cretaceous sp.				X	1
Rhagodiscus sp.				X	1

Table A30. Milano MV.

LEV7GC 40–43 Matrix					
Mixed; Mostly Oligocene–Miocene					
Species	A	C	F	R	Specimens Counted
Pleistocene					
Gephyrocapsa oceanica				X	2
Neogene					
Calcidiscus macintyrei			X		4
Coccolithus miopelagicus				X	1
Discoaster asymmetricus				X	1
Gephyrocapsa <3 μm				X	1
Helicosphaera carteri		X			7
Helicosphaera princei				X	1
Helicosphaera stalis				X	1
Pseudoemiliania lacunosa				X	2
Reticulofenestra pseudoumbilicus	X				40
Sphenolithus disbelemnos				X	2
Sphenolithus heteromorphus			X		3
Umbilicosphaera jafari		X			6
Paleogene					
Cyclicargolithus abisetus				X	2
Discoaster barbadiensis				X	1
Reticulofenestra bisecta				X	1

Reticulofenestra lockeri				X	1
Zygrhablithus bijugatus				X	1
Long-range Paleogene–Neogene					
Braarudosphaera bigelowii				X	1
Coccolithus pelagicus	X				15
Coronocyclus mesostenos				X	
Cyclicargolithus floridanus			X		4
Discoaster deflandrei				X	
Discoaster sp.			X		4
Helicosphaera mediterranea				X	1
Pontosphaera multipora				X	1
Pontosphaera sp.			X		2
Reticulofenestra perplexa				X	2
Sphenolithus moriformis			X		3
Cretaceous					
undetermined Cretaceous sp.				X	1
Dizomatolithus lehmanii			X		3
Eiffellithus turriseiffelii				X	1
Rhagodiscus sp.				X	1

Table A31. Milano MV.

LEV7GC 40–43 Clast 1					
Biozone: CNM8–9					
Species	A	C	F	R	Specimens Counted
Neogene					
Calcidiscus leptoporus			X		6
Calcidiscus macintyrei	X				12
Discoaster variabilis			X		6
Helicosphaera carteri			X		9
Helicosphaera walbersdorfensis			X		5
Reticulofenestra	X				15

pseudoumbilicus					
Sphenolithus abies			X		4
Umbilicosphaera rotula			X		4
Paleogene					
Reticulofenestra hillae				X	3
Reticulofenestra reticulata				X	1
Reticulofenestra bisecta				X	1
Zygrhablithus bijugatus				X	1
Long-range Paleogene–Neogene					
Braarudosphaera bigelowii			X		4
Coccolithus pelagicus	X				19
Cyclicargolithus floridanus				X	1
Discoaster sp.		X			8
Helicosphaera intermedia				X	1
Helicosphaera mediterranea				X	2
Pontosphaera multipora				X	2
Pontosphaera sp.				X	4
Reticulofenestra perplexa	X				15
Rhabdosphaera sp.				X	2
small reticulofenestroids	X				18
Sphenolithus moriformis			X		8
Cretaceous					
Zeugrhabdotus sp.				X	1
undetermined Cretaceous sp.				X	1

Table A32. Milano MV.

LEV7GC 40–43 Clast 2					
Biozone: CNM8–9					
Species	A	C	F	R	Specimens Counted
Neogene					
Calcidiscus leptoporus				X	2

Cryptococcolithus sp.				X	1
Discoaster variabilis				X	1
Gephyrocapsa <3 μm				X	1
Helicosphaera carteri	X				15
Helicosphaera stalis				X	1
Helicosphaera walbersdorfensis			X		6
Reticulofenestra pseudoumbilicus	X				39
Sphenolithus abies				X	2
Sphenolithus heteromorphus				X	1
Umbilicosphaera foliosa				X	1
Umbilicosphaera jafari	X				20
Paleogene					
Cruciplacolithus sp.				X	1
Reticulofenestra bisecta				X	1
Sphenolithus ciperoensis				X	1
Long-range Paleogene–Neogene					
Coccolithus pelagicus	X				15
Coronocyclus mesostenos		X			8
Cyclicargolithus floridanus	X				10
Helicosphaera intermedia				X	1
Pontosphaera multipora				X	1
Pontosphaera sp.		X			5
small reticulofenestroids	X				28
Sphenolithus moriformis			X		4

Table A33. Milano MV.

LEV7GC 78–80 Matrix					
Mixed; Mostly Oligocene–Miocene					
Species	A	C	F	R	Specimens Counted
Neogene					
Calcidiscus				X	1

macintyrei					
Helicosphaera carteri				X	2
Reticulofenestra pseudoumbilicus	X				48
Sphenolithus disbelemnos				X	2
Sphenolithus heteromorphus			X		4
Umbilicosphaera jafari		X			6
Umbilicosphaera rotula			X		3
Paleogene					
Discoaster barbadiensis				X	1
Sphenolithus distentus				X	1
Long-range Paleogene–Neogene					
Braarudosphaera bigelowii				X	1
Coccolithus pelagicus	X				21
Cyclicargolithus floridanus	X				19
Discoaster sp.		X			5
Pontosphaera multipora				X	1
Pontosphaera sp.				X	2
Reticulofenestra perplexa			X		3
small reticulofenestroids	X				10
Sphenolithus calyculus				X	1
Sphenolithus moriformis		X			5

Table A34. Milano MV.

LEV7GC 78–80 Clast 1					
Biozone: CNM8–9					
Species	A	C	F	R	Specimens Counted
Neogene					
Calcidiscus macintyrei				X	3
Coccolithus miopelagicus				X	2
Helicosphaera carteri				X	2
Reticulofenestra pseudoumbilicus	X				14
Sphenolithus abies				X	1
Sphenolithus disbelemnos				X	2
Sphenolithus heteromorphus				X	2
Umbilicosphaera foliosa			X		4
Umbilicosphaera jafari			X		2
Umbilicosphaera rotaria				X	1
Umbilicosphaera rotula				X	2
Paleogene					
Discoaster barbadiensis				X	1
Reticulofenestra bisecta				X	3
Reticulofenestra lockeri				X	3
Long-range Paleogene–Neogene					
Coccolithus pelagicus	X				12
Coronocyclus mesostenos			X		3
Cyclicargolithus floridanus		X			6
Pontosphaera sp.				X	1
small reticulofenestroids		X			48
Sphenolithus moriformis		X			8

Table A35. Milano MV.

LEV7GC 78–80 Clast 2
Biozone: undetermined

Table A36. Leipzig MV.

LEV9GC 10–13 Matrix					
Mixed; Mostly Oligocene–Miocene					
Species	A	C	F	R	Specimens Counted
Neogene					
Calcidiscus macintyrei				X	3
Helicosphaera carteri				X	2
Reticulofenestra pseudoumbilicus	X				19
Sphenolithus heteromorphus				X	1
Umbilicosphaera jafari				X	1
Umbilicosphaera rotula				X	1
Paleogene					
Discoaster saipanensis				X	1
Long-range Paleogene–Neogene					
Coccolithus pelagicus	X				14
Cyclicargolithus floridanus		X			9
Discoaster deflandrei				X	2
Discoaster sp.			X		5
Helicosphaera intermedia				X	1
Reticulofenestra perplexa				X	2
Sphenolithus moriformis			X		5
Coronocyclus mesostenos				X	2
Cretaceous					
undetermined Cretaceous sp.				X	2

Table A37. Leipzig MV.

LEV9GC 10–13

Clast 1					
Biozone: CNM8–9					
Species	A	C	F	R	Specimens Counted
Neogene					
Calcidiscus leptoporus				X	1
Calcidiscus macintyrei			X		2
Helicosphaera carteri		X			8
Helicosphaera princei				X	1
Helicosphaera stalis				X	1
Helicosphaera walbersdorfensis			X		2
Reticulofenestra pseudoumbilicus	X				25
Rhabdosphaera sp.				X	1
Sphenolithus abies				X	1
Sphenolithus cometa				X	1
Sphenolithus disbelemnos				X	2
Sphenolithus heteromorphus				X	2
Umbilicosphaera jafari			X		4
Umbilicosphaera rotula				X	1
Paleogene					
Coccolithus fomosus				X	1
Cyclicargolithus abisectus				X	1
Sphenolithus ciperoensis				X	1
Zygrhablithus bijugatus				X	1
Long-range Paleogene–Neogene					
Coccolithus pelagicus	X				37
Cyclicargolithus floridanus	X				18
Discoaster deflandrei				X	3
Discoaster sp.			X		3
Helicosphaera intermedia				X	2
Helicosphaera mediterranea				X	2
Helicosphaera sp.				X	3
Pontosphaera sp.				X	
Reticulofenestra		X			9

perplexa					
small reticulofenestroids	X				3
Sphenolithus moriformis		X			6
Cretaceous					
undetermined Cretaceous sp.				X	1
Dizomatolithus lehmanii				X	2

Table A38. Leipzig MV.

LEV9GC 67–69 Clast 1					
Biozone: CNM6–7					
Species	A	C	F	R	Specimens Counted
Neogene					
Calcidiscus macintyrei				X	1
Calcidiscus premacintyrei				X	1
Discoaster exilis				X	1
Helicosphaera ampliaperta			X		5
Helicosphaera carteri			X		4
Helicosphaera princei				X	1
Sphenolithus cometa				X	2
Sphenolithus dibelemnos				X	1
Sphenolithus heteromorphus			X		3
Umbilicosphaera jafari			X		3
Paleogene					
Cyclicargolithus abisetus				X	2
Discoaster barbadiensis				X	1
Reticulofenestra bisecta				X	1
Long-range Paleogene–Neogene					
Coccolithus pelagicus	X				10
Coronocyclus mesostenos				X	2
Cyclicargolithus floridanus	X				24
Discoaster deflandrei			X		4

Discoaster sp.				X	11
Helicosphaera intermedia				X	4
Helicosphaera mediterranea				X	1
Pontosphaera multipora				X	1
Pontosphaera sp.				X	1
Reticulofenestra perplexa				X	3
small reticulofenestroids	X				10
Sphenolithus moriformis	X				11
Sphenolithus sp.				X	1
Cretaceous					
Dizomatolithus lehmanii			X		4

Table A39. Leipzig MV.

LEV9GC 67–69 Clast 2
Biozone: undetermined

Table A40. Leipzig MV.

LEV9GC 98–100 Matrix					
Mixed; Mostly Oligocene–Miocene					
Species	A	C	F	R	Specimens Counted
Neogene					
Calcidiscus macintyrei				X	2
Helicosphaera carteri			X		4
Reticulofenestra pseudoumbilicus	X				17
Sphenolithus heteromorphus				X	2
Umbilicosphaera jafari				X	3
Paleogene					
Cyclicargolithus abisetus				X	1
Discoaster multiradiatus				X	1
Reticulofenestra hillae				X	2
Long-range Paleogene–Neogen					

e					
Braarudosphaera bigelowii				X	1
Coccolithus pelagicus	X				11
Coronocyclus mesostenos				X	1
Coronocyclus nitescens				X	1
Cyclicargolithus floridanus			X		5
Discoaster deflandrei				X	1
Discoaster sp.			X		5
Micrantholithus sp.				X	1
Pontosphaera multipora				X	1
Pontosphaera sp.				X	2
Reticulofenestra perplexa				X	2
Cretaceous					
Dizomatolithus lehmanii				X	1

Table A41. Leipzig MV.

LEV9GC 98–100 Clast 1					
Mixed; Mostly Oligocene–Miocene					
Species	A	C	F	R	Specimens Counted
Neogene					
Calcidiscus premacintyrei				X	2
Coccolithus miopelagicus				X	1
Cryptococcolithus sp.				X	1
Reticulofenestra pseudoumbilicus				X	1
Umbilicosphaera roluta				X	1
Paleogene					
Cyclicargolithus abisetus		X			4
Helicosphaera compacta			X		2
Helicosphaera recta				X	1
Reticulofenestra bisecta			X		1
Reticulofenestra erbae				X	2

Reticulofenestra hillae				X	2
Reticulofenestra lockeri				X	2
Sphenolithus distentus				X	1
Zygrhablithus bijugatus				X	1
Long-range Paleogene–Neogene					
Coccolithus pelagicus	X				13
Coronocyclus mesostenos				X	2
Coronocyclus nitescens				X	2
Cyclicargolithus floridanus	X				82
Discoaster deflandrei			X		4
Discoaster sp.				X	1
Helicosphaera intermedia		X			7
Helicosphaera sp.			X		5
Pontosphaera sp.				X	2
Reticulofenestra perplexa				X	2
small reticulofenestroids			X		10
Sphenolithus moriformis	X				9
Cretaceous					
undetermined Cretaceous sp.				X	2
Dizomatolithus lehmanii			X		4

Table A42. Leipzig MV.

LEV9GC 98–100 Clast 2					
Biozone: CNM6–7					
Species	A	C	F	R	Specimens Counted
Neogene					
Calcidiscus premacintyrei				X	2
Helicosphaera carteri		X			7
Helicosphaera walbersdorfensis			X		2
small reticulofenestroids	X				9

Sphenolithus heteromorphus	X				12
Umbilicosphaera jafari	X				22
Umbilicosphaera rotula		X			8
Helicosphaera vedderi				X	1
Discoaster variabilis				X	1
Discoaster petaliformis				X	1
Helicosphaera waltans		X			2
Helicosphaera ampliaperta			X		2
Coccolithus miopelagicus				X	5
Paleogene					
Cyclicargolithus abisectus				X	1
Long-range Paleogene–Neogene					
Coccolithus pelagicus	X				31
Cyclicargolithus floridanus	X				11
Discoaster sp.			X		3
Helicosphaera intermedia				X	1
Helicosphaera sp.		X			10
Pontosphaera sp.			X		3
Reticulofenestra perplexa			X		3
Sphenolithus moriformis		X			6

Table A43. Leipzig MV.

LEV9GC 98–100 Clast 3					
Biozone: CNM8–9					
Species	A	C	F	R	Specimens Counted
Neogene					
Calcidiscus macintyrei		X			8
Coccolithus miopelagicus				X	2
Discoaster formosus				X	1
Helicosphaera carteri				X	7
Reticulofenestra	X				31

pseudoumbilicus					
Rhabdosphaera sp.				X	2
Umbilicosphaera jafari		X			5
Umbilicosphaera rotula				X	1
Paleogene					
Cyclicargolithus abisetus				X	1
Reticulofenestra daivesi				X	1
Sphenolithus ciperoensis				X	1
Zygrhablithus bijugatus				X	1
Long-range Paleogene–Neogene					
Coccolithus pelagicus	X				28
Cyclicargolithus floridanus			X		6
Discoaster deflandrei				X	2
Discoaster sp.		X			5
Helicosphaera intermedia				X	2
Pontosphaera multipora				X	3
Pontosphaera sp.			X		3
Reticulofenestra perplexa	X				17
Sphenolithus moriformis	X				15
Cretaceous					
Eiffellithus sp.				X	1
Watznaueria barnesiae				X	2

Table A44. Leipzig MV.

LEV9GC 128–130 Matrix					
Mixed; Mostly Oligocene–Miocene					
Species	A	C	F	R	Specimens Counted
Neogene					
Calcidiscus macintyrei				X	1
Calcidiscus premacintyrei				X	1
Discoaster exilis				X	1

Discoaster ulnatus		X	1
Helicosphaera carteri	X		6
Helicosphaera walbersdorfensis		X	2
Reticulofenestra pseudoumbilicus	X		8
Sphenolithus abies		X	1
Sphenolithus cometa		X	1
Sphenolithus heteromorphus		X	1
Umbilicosphaera jafari	X		6
Paleogene			
Coccolithus formosus		X	1
Cyclicargolithus abisetus		X	1
Discoaster tanii		X	1
Reticulofenestra bisecta		X	1
Reticulofenestra hillae		X	1
Reticulofenestra lockeri		X	1
Sphenolithus delphix		X	1
Sphenolithus distentus		X	1
Long-range Paleogene–Neogene			
Coccolithus pelagicus	X		12
Coronocyclus mesostenos		X	1
Cyclicargolithus floridanus	X		16
Discoaster deflandrei		X	1
Discoaster sp.		X	1
Helicosphaera intermedia		X	1
Pontosphaera multipora		X	1
Reticulofenestra perplexa		X	3
Sphenolithus moriformis		X	3
Cretaceous			
Eiffelithus sp.		X	1
undetermined Cretaceous sp.		X	3
Watznaueria barnesiae		X	3

Watznaueria ovata				X	1

Table A45. Leipzig MV.

LEV9GC 128–130 Clast 1					
Biozone: undetermined					

Table A46. Leipzig MV.

LEV9GC 128–130 Clast 2					
Biozone: CNM7					
Species	A	C	F	R	Specimens Counted
Neogene					
Coccolithus miopelagicus		X			7
Helicosphaera carteri		X			5
Reticulofenestra pseudoumbilicus				X	1
Sphenolithus heteromorphus	X				14
Umbilicosphaera jafari		X			6
Umbilicosphaera rotula				X	2
Paleogene					
Discoaster barbadiensis				X	1
Long-range Paleogene–Neogene					
Coccolithus pelagicus	X				45
Coronocyclus nitescens				X	1
Cyclicargolithus floridanus	X				35
Discoaster deflandrei				X	2
Discoaster sp.		X			5
Helicosphaera intermedia				X	3
Micrantholithus sp.			X		4
Pontosphaera sp.		X			8
Reticulofenestra perplexa				X	3
small reticulofenestroids			X		4
Sphenolithus moriformis		X			6
Cretaceous					
Watznaueria				X	2

barnesiae					

Table A47. Leipzig MV.

LEV9GC 128–130 Clast 3					
Biozone: CNM8–9					
Species	A	C	F	R	Specimens Counted
Neogene					
Calcidiscus leptoporus				X	1
Discoaster bolli				X	1
Discoaster formosus				X	1
Discoaster variabilis				X	1
Helicosphaera carteri		X			8
Reticulofenestra pseudoumbilicus	X				28
Sphenolithus dissimilis				X	1
Umbilicosphaera foliosa				X	2
Umbilicosphaera jafari				X	3
Paleogene					
Zygrhablithus bijugatus				X	1
Long-range Paleogene–Neogene					
Coccolithus pelagicus		X			6
Cyclicargolithus floridanus				X	2
Discoaster sp.				X	3
Pontosphaera multipora				X	2
Pontosphaera sp.				X	1
Reticulofenestra perplexa				X	1
Sphenolithus moriformis			X		4
Cretaceous					
Dizomatolithus lehmanii				X	2

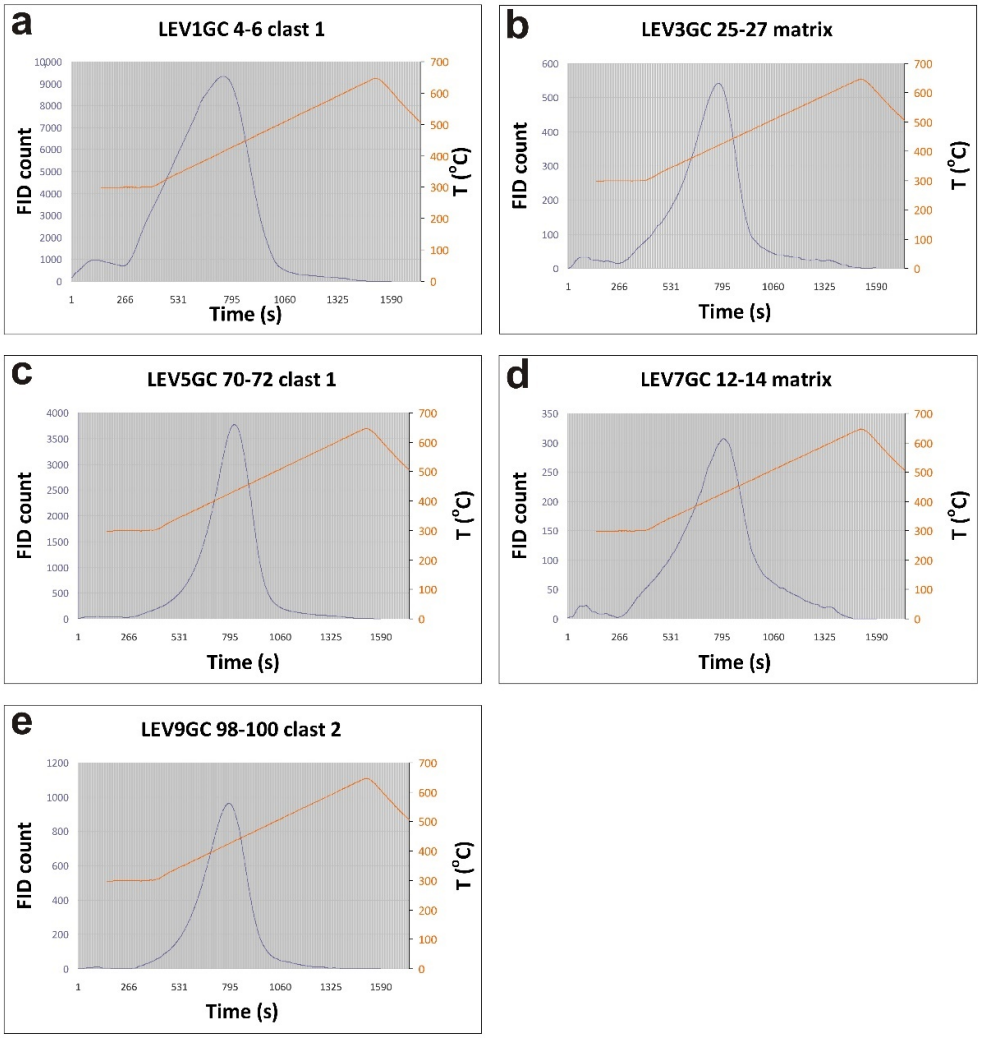

Figure A1. Distinct unimodal S2 peaks in the Rock-Eval pyrograms of samples from: (**a**) the Gelendzhik MV, (**b**) the Heraklion MV, (**c**) the Moscow MV, (**d**) the Milano MV, and (**e**) the Leipzig MV.

References

1. Limonov, A.; Woodside, J.; Cita, M.; Ivanov, M. The Mediterranean Ridge and related mud diapirism: A background. *Mar. Geol.* **1996**, *132*, 7–19, doi:10.1016/0025-3227(96)00150-8.
2. Fusi, N.; Kenyon, N.H. Distribution of mud diapirism and other geological structures from long-range sidescan sonar (GLORIA) data, in the Eastern Mediterranean Sea. *Mar. Geol.* **1996**, *132*, 21–38, doi:10.1016/0025-3227(95)00151-4.
3. Cita, M.B. Discovery of mud diapirism on the Mediterranean Ridge. A preliminary report. *Boll. Soc. Geol. Ital.* **1989**, *108*, 537–543.
4. Rabaute, A.; Chamot-Rooke, N. Quantitative mapping of active mud volcanism at the western Mediterranean Ridge-backstop contact. *Mar. Geophys. Res.* **2007**, *28*, 271–295, doi:10.1007/s11001-007-9031-8.
5. Mascle, J.; Mary, F.; Praeg, D.; Brosolo, L.; Camera, L.; Ceramicola, S.; Dupré, S. Distribution and geological control of mud volcanoes and other fluid/free gas seepage features in the Mediterranean Sea and nearby Gulf of Cadiz. *Geo Marine Lett.* **2014**, *34*, 89–110, doi:10.1007/s00367-014-0356-4.
6. Emeis, K.-C.; Robertson, A.H.F.; Richter, C.; Camerlenghi, A. (Eds.) Shipboard Scientific Party. Site 970. In *Initial Reports, 160, Proceedings of the Ocean Drilling Project (ODP)*; Ocean Drilling Program: College Station, TX, USA, 1996; Chapter 11, 377–413, doi:10.2973/odp.proc.ir.160.111.1996.
7. Emeis, K.-C.; Robertson, A.H.F.; Richter, C.; Camerlenghi, A. (Eds.) Shipboard Scientific Party. Site 971. In *Initial Reports, 160, Proceedings of the Ocean Drilling Project (ODP)*; Ocean Drilling Program: College Station, TX, USA, 1996; Chapter 12, 415–450, doi:10.2973/odp.proc.ir.160.112.1996.

8. Akhmanov, G.G. Lithology of mud breccia clasts from the Mediterranean Ridge. *Mar. Geol.* **1996**, *132*, 151–164, doi:10.1016/0025-3227(95)00158-1.
9. Schulz, H.-M.; Emeis, K.-C.; Volkmann, N. Organic carbon provenance and maturity in the mud breccia from the Napoli mud volcano: Indicators of origin and burial depth. *Earth Planet. Sci. Lett.* **1997**, *147*, 141–151, doi:10.1016/s0012-821x(97)00013-7.
10. Kopf, A.; Robertson, A.; Volkmann, N. Origin of mud breccia from the Mediterranean Ridge accretionary complex based on evidence of the maturity of organic matter and related petrographic and regional tectonic evidence. *Mar. Geol.* **2000**, *166*, 65–82, doi:10.1016/s0025-3227(00)00009-8.
11. Aloisi, G.; Pierre, C.; Rouchy, J.-M.; Foucher, J.-P.; Woodside, J. Methane-related authigenic carbonates of eastern Mediterranean Sea mud volcanoes and their possible relation to gas hydrate destabilisation. *Earth Planet. Sci. Lett.* **2000**, *184*, 321–338, doi:10.1016/s0012-821x(00)00322-8.
12. Woodside, J.M.; Ivanov, M.K.; Limonov, A.F. Shallow gas and gas hydrates in the Anaximander Mountains region, eastern Mediterranean Sea. *Geol. Soc. Lond. Spéc. Publ.* **1998**, *137*, 177–193, doi:10.1144/gsl.sp.1998.137.01.15.
13. Woodside, J.M.; Ivanov, M.K.; Limonov, A.F. *Neotectonics and Fluid Flow through Seafloor Sediments in the Eastern Mediterranean and Black Seas, Parts I and II*; Technical Series No. 48; UNESCO, Intergovernmental Oceanographic Commission: Paris, France, 1997.
14. Perissoratis, C.; Ioakim, C.; Alexandri, S.; Woodside, J.; Nomikou, P.; Dählmann, A.; Casas, D.; Heeschen, K.; Amman, H.; Rousakis, G.; et al. Thessaloniki Mud Volcano, the Shallowest Gas Hydrate-Bearing Mud Volcano in the Anaximander Mountains, Eastern Mediterranean. *J. Geol. Res.* **2011**, *2011*, 1–11, doi:10.1155/2011/247983.
15. Pape, T.; Kasten, S.; Zabel, M.; Bahr, A.; Abegg, F.; Hohnberg, H.-J.; Bohrmann, G. Gas hydrates in shallow deposits of the Amsterdam mud volcano, Anaximander Mountains, Northeastern Mediterranean Sea. *Geo-Marine Lett.* **2010**, *30*, 187–206, doi:10.1007/s00367-010-0197-8.
16. Mascle, J.; Mascle, G. *Geological and Morphotectonic Map of the Mediterranean Donain, 2012*; Commission de la Carte Geologique du Monde (UNESCO): Paris, France, 2012.
17. Cita, M.B.; Ryan, W.F.B.; Paggi, L. Prometheus mud breccia: An example of shale diapirism in the western Mediterranean ridge. *Ann. Geol. Pays Hell.* **1981**, *30*, 543–570.
18. Camerlenghi, A.; Cita, M.; Hieke, W.; Ricchiuto, T. Geological evidence for mud diapirism on the Mediterranean Ridge accretionary complex. *Earth Planet. Sci. Lett.* **1992**, *109*, 493–504, doi:10.1016/0012-821x(92)90109-9.
19. Papanikolaou, D. Tectonostratigraphic models of the Alpine terranes and subduction history of the Hellenides. *Tectonophysics* **2013**, *595–596*, 1–24, doi:10.1016/j.tecto.2012.08.008.
20. Papanikolaou, D. Timing of tectonic emplacement of the ophiolites and terrane paleogeography in the Hellenides. *Lithos* **2009**, *108*, 262–280, doi:10.1016/j.lithos.2008.08.003.
21. Fassoulas, C.; Kilias, A.; Mountrakis, D. Postnappe stacking extension and exhumation of high-pressure/low-temperature rocks in the island of Crete, Greece. *Tectonics* **1994**, *13*, 127–138, doi:10.1029/93tc01955.
22. Papanikolaou, D.; Vassilakis, E. Thrust faults and extensional detachment faults in Cretan tectono-stratigraphy: Implications for Middle Miocene extension. *Tectonophys.* **2010**, *488*, 233–247, doi:10.1016/j.tecto.2009.06.024.
23. Mountrakis, D. Tectonic evolution of the Hellenic orogen: Geometry and kinematics of deformation. *Bull. Geol. Soc. Greece* **2002**, *34*, 2113–2126.
24. Kilias, A.; Fassoulas, C.; Mountrakis, D. Tertiary extension of continental crust and uplift of Psiloritis metamorphic core complex in the central part of the Hellenic Arc (Crete, Greece). *Act. Cont. Margins Present Past* **1994**, *28*, 417–430, doi:10.1007/978-3-662-38521-0_16.
25. Robertson, A.; Kopf, A. Tectonic setting and processes of mud volcanism on the Mediterranean Ridge accretionary complex: Evidence from Leg 160. *Proc. Ocean Drill. Program 160 Sci. Results* **1998**, *160*, 50, doi:10.2973/odp.proc.sr.160.062.1998.
26. Panagiotopoulos, I.P.; Paraschos, F.; Rousakis, G.; Hatzianestis, I.; Parinos, C.; Morfis, I.; Gogou, A. Assessment of the eruptive activity and identification of the mud breccia's source in the Olimpi mud volcano field, Eastern Mediterranean. *Deep Sea Res. Part II Top. Stud. Oceanogr.* **2020**, *171*, 104701.
27. Cita, M.; Erba, E.; Lucchi, R.G.; Pott, M.; Van Der Meer, R.; Nieto, L. Stratigraphy and sedimentation in the Mediterranean Ridge diapiric belt. *Mar. Geol.* **1996**, *132*, 131–150, doi:10.1016/0025-3227(96)00157-0.
28. Bown, P.R.; Young, J.R. Introduction—calcareous nannoplankton biology. In *Calcareous Nannofossil Biostratigraphy*; Bown, P.R., Ed.; British Micropalaeontological Society Publication Series: Birmingham, UK, 1998; pp. 1–15.
29. Marsaglia, K.; Tentori, D.; Milliken, K.; Leckie, R.M.; Doran, L. IODP digital reference for smear slide analysis of marine mud—Part 2: Methodology and Atlas of biogenic components. In Proceedings of the Organic-Rich Mud Rocks: Geochemistry, Physical Properties, and Paleo-Environments (posters), Geological Society of America Annual Meeting, Vancouver, BC, Canada, 19–22 October 2014.
30. Agnini, C.; Monechi, S.; Raffi, I. Calcareous nannofossil biostratigraphy: Historical background and application in Cenozoic chronostratigraphy. *Lethaia* **2017**, *50*, 447–463, doi:10.1111/let.12218.
31. Backman, J.; Raffi, I.; Rio, D.; Fornaciari, E.; Pälike, H. Biozonation and biochronology of Miocene through Pleistocene calcareous nannofossils from low and middle latitudes. *Newsletters Strat.* **2012**, *45*, 221–244, doi:10.1127/0078-0421/2012/0022.
32. Martini, E. Standard Tertiary and Quaternary calcareous nannoplankton zonation. In *Proceedings of the 2nd Planktonic Conference, Roma, Italy*, 1970; Farrinacy, A., Ed.; Tecnoscienza: Rome, Italy, 1971; Volume 2, pp. 739–785.

33. Espitalie, J.; Laporte, J.L.; Madec, M.; Marquis, F.; Leplat, P.; Paulet, J.; Boutefeu, A. Rapid method for source rocks characterization and for determination of petroleum potential and degree of evolution. *Rev. Inst. Fr. Pet.* **1977**, *32*, 23–42.
34. Espitalie, J.; Madec, M.; Tissot, B.P.; Mennig, J.; Leplat, P. Source Rock Characterization Method for Petroleum Exploration. In Proceedings of the Offshore Technology Conference, Houston, TX, USA, 1–4 May 1977.
35. Tissot, B.P.; Welte, D.H. *Petroleum Formation and Occurrence*, 2nd ed.; Springer: New York, NY, USA, 1984.
36. Emeis, K.-C.; Kvenvolden, K. Shipboard Organic Geochemistry on JOIDES Resolution. *Shipboard Org. Geochem. JOIDES Resolut.* **1986**, doi:10.2973/odp.tn.7.1986.
37. Espitalie, J.; DeRoo, G.; Marquis, F. La pyrolyse Rock-Eval et ses applications. Deuxième partie. *Rev. l'Institut Français du Pétrole* **1985**, *40*, 755–784, doi:10.2516/ogst:1985045.
38. Hunt, J.M. *Petroleum Geochemistry and Geology*; W.H. Freeman: New York, NY, USA, 1995.
39. Jackson, K.; Hawkins, P.; Bennett, A. Regional Facies and Geochemical Evaluation of the Southern Denison trough, Queensland. *APPEA J.* **1980**, *20*, 143–158, doi:10.1071/aj79013.
40. Jiang, C.; Chen, Z.; Lavoie, D.; Percival, J.B.; Kabanov, P. Mineral carbon MinC(%) from Rock-Eval analysis as a reliable and cost-effective measurement of carbonate contents in shale source and reservoir rocks. *Mar. Pet. Geol.* **2017**, *83*, 184–194, doi:10.1016/j.marpetgeo.2017.03.017.
41. Staffini, F.; Spezzaferri, S.; Aghib, F. Mud diapirs of the Mediterranean Ridge: Sedimentological and micropaleontological study of the mud breccia. *Riv. Ital. Paleontol. Stratigr.* **1993**, *99*, 225–254.
42. Limonov, A.F.; Woodside, J.M.; Ivanov, M.K. *Mud Volcanism in the Mediterranean and Black Seas and Shallow Structure of the Eratosthenes Seamount: Initial Results of the Geological and Geophysical Investigations during the 3rd UNESCO-ESF "Training-Through-Research" Cruise of RV Gelendzhik (June–July 1993)*; UNESCO Reports in Marine Science: Paris, France, 1994; p. 171.
43. Silva, I.P.; Erba, E.; Spezzaferri, S.; Cita, M.B. Age variation in the source of the diapiric mud breccia along and across the axis of the Mediterranean Ridge Accretionary Complex. *Mar. Geol.* **1996**, *132*, 175–202, doi:10.1016/0025-3227(95)00160-3.
44. Sotiropoulos, S.; Triantaphyllou, M.V.; Kamberis, E.; Tsaila-Monopolis, S. Paleogene terrigenous (flysch) sequences in Etoloakarnania region (W. Greece). Plankton stratigraphy and paleoenvironmental implications. *Geobios* **2008**, *41*, 415–433, doi:10.1016/j.geobios.2007.10.007.
45. Triantaphyllou, M.V. Calcareous nannofossil dating of Ionian and Gavrovo flysch deposits in the External Hellenides Carbonate Platform (Greece): Overview and implications. *Tectonophys.* **2013**, *595-596*, 235–249, doi:10.1016/j.tecto.2012.05.007.
46. Triantaphyllou, M. A review of Cenozoic calcareous nannofossil biostratigraphic studies in the Hellenic territory (Greece): Achievements and limitations. INA16 Abstracts. *J. Nannoplankton Res.* **2017**, *37*, 127.
47. Lagaria, A.; Mandalakis, M.; Mara, P.; Frangoulis, C.; Karatsolis, B.-T.; Pitta, P.; Triantaphyllou, M.; Tsiola, A.; Psarra, S. Phytoplankton variability and community structure in relation to hydrographic features in the NE Aegean frontal area (NE Mediterranean Sea). *Cont. Shelf Res.* **2017**, *149*, 124–137, doi:10.1016/j.csr.2016.07.014.
48. Rohling, E.; Marino, G.; Grant, K. Mediterranean climate and oceanography, and the periodic development of anoxic events (sapropels). *Earth-Sci. Rev.* **2015**, *143*, 62–97, doi:10.1016/j.earscirev.2015.01.008.
49. Triantaphyllou, M.; Ziveri, P.; Gogou, A.; Marino, G.; Lykousis, V.; Bouloubassi, I.; Emeis, K.-C.; Kouli, K.; Dimiza, M.; Rosell-Melé, A.; et al. Late Glacial–Holocene climate variability at the south-eastern margin of the Aegean Sea. *Mar. Geol.* **2009**, *266*, 182–197, doi:10.1016/j.margeo.2009.08.005.
50. Triantaphyllou, M.V.; Gogou, A.; Dimiza, M.D.; Kostopoulou, S.; Parinos, C.; Roussakis, G.; Geraga, M.; Bouloubassi, I.; Fleitmann, D.; Zervakis, V.; et al. Holocene Climatic Optimum centennial-scale paleoceanography in the NE Aegean (Mediterranean Sea). *Geo-Mar. Lett.* **2016**, *36*, 51–66, doi:10.1007/s00367-015-0426-2.
51. Taylforth, J.E.; McCay, G.A.; Ellam, R.; Raffi, I.; Kroon, D.; Robertson, A.H. Middle Miocene (Langhian) sapropel formation in the easternmost Mediterranean deep-water basin: Evidence from northern Cyprus. *Mar. Pet. Geol.* **2014**, *57*, 521–536, doi:10.1016/j.marpetgeo.2014.04.015.
52. Athanasiou, M.; Triantaphyllou, M.; Dimiza, M.; Gogou, A.; Bouloubassi, I.; Tsiolakis, E.; Theodorou, G. Early-Middle Miocene from Kotaphi hill section (Nicosia, Cyprus): Preliminary biostratigraphy and paleoceanographic implications. *Bull. Geol. Soc. Greece* **2016**, *47*, 62, doi:10.12681/bgsg.10899.
53. Athanasiou, M.; Triantaphyllou, M.V.; Dimiza, M.D.; Gogou, A.; Panagiotopoulos, I.; Arabas, A.; Skampa, E.; Kouli, K.; Hatzaki, M.; Tsiolakis, E. Reconstruction of oceanographic and environmental conditions in the eastern Mediterranean (Kottafi Hill section, Cyprus Island) during the middle Miocene Climate Transition. *Rev. Micropaleontol.* **2021**, *70*, 100480.
54. Kidd, R.B.; Cita, M.B.; Ryan, W.B.F. Stratigraphy of eastern Mediterranean sapropel sequences recovered during DSDP Leg 42A and their paleoenvironmental significance. *Affil. Lamont-Doherty Geol. Obs*. **1978**, *42*, 421.
55. Athanasiou, M.; Bouloubassi, I.; Gogou, A.; Klein, V.; Dimiza, M.D.; Parinos, C.; Skampa, E.; Triantaphyllou, M.V. Sea surface temperatures and environmental conditions during the "warm Pliocene" interval (~4.1–3.2 Ma) in the Eastern Mediterranean (Cyprus). *Glob. Planet. Chang.* **2017**, *150*, 46–57.
56. Manta, K.; Rousakis, G.; Anastasakis, G.; Lykousis, V.; Sakellariou, D.; Panagiotopoulos, I.P. Sediment transport mechanisms from the slopes and canyons to the deep basins south of Crete Island (southeast Mediterranean). *Geo-Mar. Lett.* **2019**, *39*, 295–312, doi:10.1007/s00367-019-00575-1.
57. Killops, S.D.; Killops, V.J. *Introduction to Organic Geochemistry*, 2nd ed.; Wiley-Blackwell: Hoboken, NJ, USA, 2013.
58. Peters, K.E. Guidelines for Evaluating Petroleum Source Rock using Programmed Pyrolysis. *AAPG Bull.* **1986**, *70*, 318–329, doi:10.1306/94885688-1704-11d7-8645000102c1865d.

59. Kozlova, E.; Ivanov, M.K.; Baudin, F.; Largeau, C.; Derenne, S. Composition and maturity of organic matter in the rock clasts of mud volcanic breccia. North Atlantic and Labrador Sea Margin Architecture and Sedimentary Process. In *International Conference and 12th Post-Cruise Meeting of the Training-Trough-Research Programme, Copenhagen, Denmark, 2004*; UNESCO—Intergovernmental Oceanographic Commission: Paris, France, 2004; Volume 191, pp. 24–25.
60. Yang, S.; Horsfield, B. Critical review of the uncertainty of Tmax in revealing the thermal maturity of organic matter in sedimentary rocks. *Int. J. Coal Geol.* **2020**, *225*, 103500, doi:10.1016/j.coal.2020.103500.